Field measurements of incision rates following bedrock exposure: Implications for process controls on the long profiles of valleys cut by rivers and debris flows

Jonathan D. Stock†
Department of Earth and Planetary Science, University of California, Berkeley, California 94720, USA

David R. Montgomery
Brian D. Collins
Department of Earth and Space Sciences, University of Washington, Seattle, Washington 98195, USA

William E. Dietrich
Leonard Sklar‡
Department of Earth and Planetary Science, University of California, Berkeley, California 94720, USA

ABSTRACT

Until recently, published rates of incision of bedrock valleys came from indirect dating of incised surfaces. A small but growing literature based on direct measurement reports short-term bedrock lowering at geologically unsustainable rates. We report observations of bedrock lowering from erosion pins monitored over 1–7 yr in 10 valleys that cut indurated volcanic and sedimentary rocks in Washington, Oregon, California, and Taiwan. Most of these channels have historically been stripped of sediment. Their bedrock is exposed to bed-load abrasion, plucking, and seasonal wetting and drying that comminutes hard, intact rock into plates or equant fragments that are removed by higher flows. Consequent incision rates are proportional to the square of rock tensile strength, in agreement with experimental results of others. Measured rates up to centimeters per year far exceed regional long-term erosion-rate estimates, even for apparently minor sediment-transport rates. Cultural artifacts on adjoining strath terraces in Washington and Taiwan indicate at least several decades of lowering at these extreme rates. Lacking sediment cover, lithologies at these sites lower at rates that far exceed long-term rock-uplift rates. This rate disparity makes it unlikely that the long profiles of these rivers are directly adjusted to either bedrock hardness or rock-uplift rate in the manner predicted by the stream power law, despite the observation that their profiles are well fit by power-law plots of drainage area vs. slope. We hypothesize that the threshold of motion of a thin sediment mantle, rather than bedrock hardness or rock-uplift rate, controls channel slope in weak bedrock lithologies with tensile strengths below ~3–5 MPa. To illustrate this hypothesis and to provide an alternative interpretation for power-law plots of area vs. slope, we combine Shields' threshold transport concept with measured hydraulic relationships and downstream fining rates. In contrast to fluvial reaches, none of the hundreds of erosion pins we installed in steep valleys recently scoured to bedrock by debris flows indicate any postevent fluvial lowering. These results are consistent with episodic debris flows as the primary agent of bedrock lowering in the steepest parts of the channel network above ~0.03–0.10 slope.

Keywords: geomorphology, erosion, neotectonics, rivers, weathering.

STATEMENT OF THE PROBLEM

Over the last two decades, a model for long-term river incision into bedrock has emerged that proposes that lowering rates depend on rock erodibility and either local shear stress or stream power per unit bed area (e.g., Howard and Kerby, 1983; Seidl and Dietrich, 1992; Sklar and Dietrich, 1998; Stock and Montgomery, 1999; Whipple and Tucker, 1999, 2002; Whipple et al., 2000; Tucker and Whipple, 2002). Substituting drainage area for discharge and channel width, this theory predicts that when rock-uplift rates (U) are balanced with incision, local channel slope S varies as a power law with drainage area A and rock erodibility K:

$$S = (U/K)^{1/n} A^{-m/n}, \quad (1)$$

where m and n are exponents in the incision law, whose values are debated (Seidl and Dietrich, 1992; Seidl et al., 1994; Tucker and Slingerland, 1996; Stock and Montgomery, 1999; Whipple and Tucker, 1999; Whipple et al., 2000). The intercept of this power law depends on the ratio of rock-uplift rate to a measure of rock erodibility. For instance, Snyder et al. (2000) have proposed that mapping the spatial variation of this ratio can be used to infer spatial patterns of rock-uplift rate. The stream power law is widely used to model incision in steepland valleys (e.g., Anderson, 1994; Whipple and Tucker, 1999; Whipple et al., 1999; Davy and Crave, 2000; Willett et al., 2001; Baldwin et al., 2003; Kirby et al., 2003). Recent adaptations include a threshold stress value (e.g., Lave and Avouac, 2001; Baldwin et al., 2003) and inclusion of the effects of sediment supply (Sklar and Dietrich, 1998; Whipple and Tucker, 2002). A substantial number of river basins can be characterized by log–log-linear plots of drainage area against slope (e.g., Fig. 1), a finding that appears consistent with the application of Equation 1. Field

†Present address: U.S. Geological Survey, Menlo Park, California, USA; e-mail: jstock@usgs.gov.
‡Present address: Department of Geosciences, San Francisco State University, San Francisco, California, USA.

GSA Bulletin; January/February 2005; v. 117; no. 11/12; p. 174–194; doi: 10.1130/B25560.1; 16 figures; 3 tables.

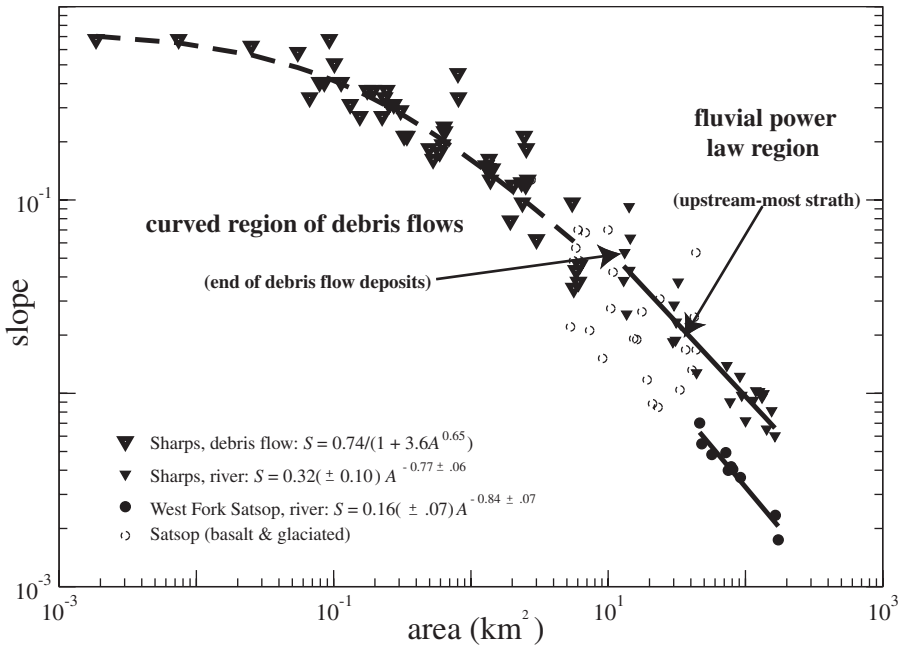

Figure 1. Area vs. slope plot for W.F. Satsop, in sandstones of the peripheral Olympic Mountains, Washington, and Sharps Creek in volcaniclastic rocks of the Oregon Cascades. Data from source 7.5′ contour maps, measured by hand. Power-law fits weighted by inverse slope and standard errors for parameters shown. Uncertainties for W.F. Satsop, intercept shown as a range. Curved debris-flow region extracted by using threshold curvature of 0.001 on the 2nd derivative of equation in the legend (see also Stock and Dietrich, 2003).

and modeling studies (e.g., Howard and Kerby, 1983; Seidl and Dietrich, 1992; Stock and Montgomery, 1999; Whipple et al., 2000) also appear consistent with its use in some rivers. Implicit in its use is the notion that at some time scale, the rock substrate is resistant enough to remain exposed as the long profile steepens toward a new equilibrium at higher rock-uplift rates. This is one of the adjustments that separate bedrock longitudinal-profile models from transport-limited models (e.g., Tucker and Slingerland, 1996; Gasparini et al., 1999). However, if certain lithologies can wear at short-term rates that far exceed rock-uplift rates, this adjustment cannot occur. In such a case it would be difficult to understand how such long profiles are adjusted to rock strength or rock-uplift rate in the simple way predicted by Equation 1.

Two recent discoveries suggest that the simple stream power law is incomplete and even wrong for certain parts of valley networks. First, map-derived and high-resolution longitudinal profiles show a clear deviation from the power-law prediction at slopes of >0.03–0.10 (e.g., Fig. 1; Seidl and Dietrich, 1992; Montgomery and Foufoula-Georgiou, 1993; Stock and Dietrich, 2003). Field evidence indicates that on these steeper slopes, scour by episodic debris flows predominates, leading to a nonlinear plot of log S against log A (Stock and Dietrich, 2003). Consequently, in steeplands that generate debris flows, relief may be largely controlled by debris-flow incision. The boundary between fluvial and debris-flow processes, as well as the contribution of intermittent fluvial incision in the debris-flow–dominated part of the channel network, remain unexplored. As a result, there is ambiguity as to whether the curved signature of the area vs. slope plot arises solely from the action of debris flows or from a combination of fluvial and debris-flow processes interacting with weathering.

The second discovery is that for a given rock-uplift rate, sediment grain size and supply rather than rock erodibility may strongly control local channel slope. Numerical modeling (Sklar and Dietrich, 1998) and analog physical modeling (Sklar and Dietrich, 2001) demonstrate that sediment supply and size distribution influence bedrock incision by (1) providing tools of varying effectiveness for wear, and (2) creating bed coverage that prevents wear. A tradeoff between these two processes leads to a humped relationship between sediment supply and wear, such that wear initially increases with supply until bed cover begins to reduce wear at high supply rates. Sklar and Dietrich (2001) proposed that the extent of coverage may vary with tectonics and climate and that grain size may be more important than rock erodibility in setting channel gradients. Thus it is not clear that concavity of the channels in Figure 1 can be interpreted directly in terms of Equation 1. The interpretation of concavity from such plots is further complicated by Sklar and Dietrich's (2001) finding that rock erodibility varies as the square of tensile strength in laboratory experiments, leading to the possibility that some lithologies can lower at rates in excess of even high long-term rock-uplift rates (e.g., 1 cm/yr). If so, higher short-term bedrock-incision rates may be decoupled from longer-term boundary lowering rates, and the stream power law may be an inappropriate model of long-term bedrock-incision rates for certain lithologies.

We explore the implications of these two new discoveries using erosion pins to document the lowering rate of exposed valley-floor bedrock in western North America and Taiwan. In 10 rivers, and in three steepland valleys eroded by recent debris flows (we use recent to describe events that occurred within several years of our visits to sites), we installed and monitored several thousand pins over varying periods from 1994–2002. We use lowering rates measured from the pins to resolve both the issue of the influence of intermittent fluvial incision along debris-flow runouts and the question of whether these bedrock-floored streams are lowering at rates greater than regional long-term estimates. We measured long-profile drainage area and slope in valleys with these monitoring sites to investigate potential topographic signatures for both debris-flow and fluvial bedrock incision.

FIELD SITES

On an opportunistic basis, we selected channels in the western United States and Taiwan (Table 1; see Stock, 2004, for site-location maps) where we observed evidence for rapid, measurable bedrock weathering and erosion of the valley floor. In Figure 2, bedrock breakdown is associated with pervasive seasonal fracturing of weakly cemented siltstones and sandstones exposed to wetting and drying. Field observations of pervasively fractured river cobbles (Mugridge and Young, 1983) and landslide surfaces (Fujiwara, 1970) indicate rapid bedrock-weathering processes similar to those in Figure 2. An extensive geotechnical literature describes both field and laboratory evidence for the comminution of rock by such processes during wetting and drying (e.g., Taylor and Smith, 1986; Taylor and Cripps, 1987; Dick and Shakoor, 1992; Santi and Shakoor, 1997). For instance, laboratory experiments designed to simulate natural exposure to rain/sun record the

TABLE 1. FIELD DATA FOR SITES WITH EROSION PINS

Region and streams	Lithology	Tensile strength (MPa)	Slake durability	Slope	Area (km^2)	$Q_{lf\ field}$ (m^3/s)	Valley width (m)	Channel width (m)	D_{max} (m)	D_{50} (mm)
Olympics, Washington										
West Fork, Satsop	Micaceous fine ss, siltstone	0.214 (0.008)	1	0.023	121	~10	~100	22	1.1	*~40*
Lower West Fork (1)	siltstone	NC	1	0.015	150	"	~120	*~20*	*~1.5*	NC
Lower West Fork (2)	siltstone	NC	1	0.015	150	"	~120	*~20*	*~1.5*	NC
Black Creek	Micaceous med. ss	0.267 (0.033)	2	0.060	14.7	0.18	18	18	~1	40
Cascades, Washington										
Teanaway (1)	Micaceous med. ss	0.908(0.041)	NC	0.008	101	0.1–0.25	~200	25	NC	NC
Teanaway (2)	Micaceous med. ss	"	NC	0.008	101	"	~200	15	NC	NC
Teanaway (3)	Micaceous med. ss	"	NC	0.008	101	"	~200	22	NC	NC
Cascades, Oregon										
Walker (1)	Indurated lahar	2.15 (0.29)	~40–900	0.08	3.22	0.016	10	10	0.19	5
Walker (2)	Indurated lahar	"	"	0.09	3.15	*~0.01*	14	5	0.24	*~5*
Walker (3)	Indurated lahar	"	"	0.08	3.00	"	18	6	0.23	*~5*
Walker (4)	Indurated rhyolite ash-flow	NC	NT	0.14	2.41	"	13	6	~0.2	*~5*
Oregon Coast Range										
Sullivan (1)	Micaceous med. ss	4.33 (0.45)	~1000 –	0.13	3.13	~0.5	10	10	0.36	25
Sullivan (2)	Micaceous med. ss	"	1700	0.07	3.56	"	14	14	0.65	25
Sullivan tributary	Micaceous med. ss	"	"	0.1–0.8	10^{-3}–10^{-1}	0	3 – 9	-	0	-
Marlow Creek tributary 1	Micaceous med. ss	"	"	0.10–0.45	10^{-3}–10^{-2}	0	3 – 5	-	0	-
Marlow Creek tributary 2	Micaceous med. ss	"	"	0.04–0.80	10^{-3}–10^{-2}	0	3 – 5	-	0	-
California Coast Range										
South Fork, Eel	Siltstone	2.68 (0.12)	NT	0.014	114	0.1–0.2	~165	20	*~0.7*	90
Taiwan, Western Foothills										
Tachia	Siltstone, shale	0.28 (0.015)	1	0.013	1128	NC	~1170	104	4<	NC
Tali	Shale, siltstone, ss	0.14 (0.044)	1	0.019	20.36	NC	unconfined	16	1.6<	89
Tsao-Hu	Shale	NC	1	0.012	12.90	NC	unconfined	19	0.70<	60
Chang-Ping	Shale, siltsone, ss	NC	1	0.033	49.10	NC	unconfined	12	2.3<	87

Note: $Q_{lf\ field}$ is estimate of base flow at visit; italics indicate order-of-magnitude estimate from measurement elsewhere; NC—not collected; NT—not tested. Numbers in parentheses in region column indicate cross sections, increasing downstream. Slopes from reach measurement with hand-level or laser. Peak flows over monitoring period estimated from recent stage indicators. Valley width estimated by the shortest distance between opposite hillslopes in the field or on a map. Channel width is distance between banks, or distance between high-flow stage indicators if banks are absent. D_{max} is maximum flow depth along pin cross section of high-stage flow. D_{50} is median gravel diameter, estimated by using random-walk method except for Walker Creek (sieve analysis). Slake durability is defined as the number of wet/dry cycles at which the sample loses 75% of its initial dry weight.

Figure 2. Pervasive fracturing of a sandstone boulder above a base-flow waterline in the W.F. Satsop, northwest Washington. Fractured rock, commonly 10–50 mm deep, is removed from exposed surfaces by seasonal high flows, but is regenerated during spring and summer desiccation. Others have hypothesized that such features are generated by weathering during cycles of wetting and drying (see text for references).

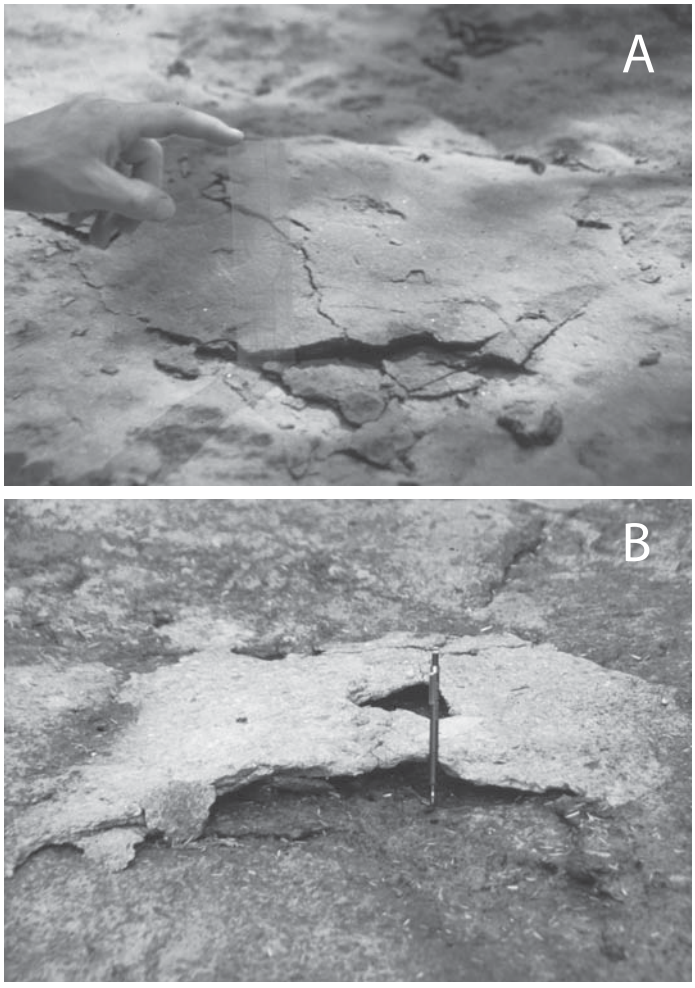

Figure 3. Tented folia in (A) micaceous sandstones in the Oregon Coast Range (Sullivan Creek) and (B) clay-rich volcanic tuff in the Oregon Cascades (Walker Creek). Both formed within several months of bedrock exposure following prolonged burial. Tented folia tend to occur preferentially above base flow and are arguably a result of weathering during cycles of wetting and drying. These tented folia represent centimeters of lowering and are commonly tens of centimeters in area.

breakdown of basalts (Haskins and Bell, 1995) and sedimentary rocks (Mugridge and Young, 1983; Yamaguchi et al., 1988; Day, 1994; Moon and Beattie, 1995; Miscevic, 1998) over 1–20 cycles of wetting and drying. Rocks containing expandable clays (especially smectites) or zeolites are most commonly observed to fracture rapidly during wetting/drying, so many of the references cited above explain the phenomenon as a result of (1) air breakage in voids or (2) mineral swelling or shrinking. In the first process, suction pressures of air voids in the interior create large tensional stresses that break mineral bonds, leading to cracks. In the second, contraction of the rock during the drying phase creates similar tensional stresses that break mineral bonds. Expansion during rehydration then leads to comminution. Measurements showing that rock cohesion decreases with repeated wetting and drying (Kusumi et al., 1998) are consistent with this hypothesis. The volumetric percentage of clay is a reasonable parameter controlling the magnitude of swelling (e.g., Dick and Shakoor, 1992; Moon and Beattie, 1995), and cementation and local sedimentary or igneous structures are thought to influence the response as well.

By contrast, in well-cemented sandstones and volcanic rocks elsewhere, we observed weathering features like those in Figure 3, skins of rock that are tens of centimeters in planform dimension and commonly one to several centimeters thick. Thin sections of these features indicate that unlike weathering rinds, their matrix materials ($CaCO_3$ or silica) are intact, and secondary porosity is limited to planes that mimic the local free surface, but are not bedding. The origin of these features remains unexplained, although their genesis may be related to hydration processes described above. To avoid confusion with the large literature on weathering rinds, we use the term "folia" (plural of "folio," Latin for "leaf") to describe the features in Figure 3.

Using features shown in Figures 2 and 3 as a guide, we selected exposed bedrock reaches with either active fluvial transport or recent debris-flow scour. Site selection is consequently biased toward steep bedrock-floored channels that transport sediment that is gravel or coarser and cut sedimentary or volcanic rocks in active tectonic settings. At each site, we installed erosion pins to test whether weathering features are seasonally formed and to document any resulting lowering. For this reason, our sites are biased toward weak lithologies that weather rapidly. Where possible, we collected bedrock samples to test whether erosion rates varied with tensile strength, as shown in flume experiments by Sklar and Dietrich (2001). At each pin-installation site (and selected surrounding basins in similar bedrock) we characterized valley longitudinal profiles through the use of area vs. slope plots. We separated longitudinal profiles into fluvial-dominated and debris-flow–dominated reaches on the basis of local field observations of processes and analysis of the area vs. slope plots for topographic signatures of fluvial (log–log-linear) and debris-flow (log-log curved) incision (Stock and Dietrich, 2003).

Olympic Mountains, Washington

Measurements from 1994 to 1996 (Stock et al., 1996) indicated rapid weathering and erosion of sedimentary rocks exposed in channels on the southern margin of the Olympic Mountains, Washington. Here the W.F. Satsop (West Fork of the Satsop River) exits the steeplands of Eocene Crescent basalts into lowlands of Eocene through Miocene marine sedimentary rocks that unconformably overlie the basalt. Sandstone and siltstone of an unnamed Eocene marine unit are the oldest of these marine sedimentary rocks and crop out in a narrow (<2 km wide) belt coincident with the abrupt mountain front. They are overlain by upper Eocene and Oligocene marine sandstone and siltstone of the Lincoln Creek Formation (Tabor and Cady, 1978) and, further downstream, by upper Miocene sandstones and siltstones of the Montesano Formation. Scattered outcrops of sandstone and siltstone of the Miocene Astoria Formation are also present. A fission-track study by Brandon et al. (1998) indicates Neogene exhumation rates of <1 mm/yr in the metasedimentary

Figure 4. Cross sections for (A) W.F. Satsop, and (B) Black Creek, Olympic Mountains, Washington, (C) Walker Creek (site 1), Oregon Cascades, and (D) S.F. Eel California Coast Range. White tape indicates cross section of erosion pins; see Table 1 for site details. Note that sites A–C are in basins that have been heavily logged.

core of the Olympics that diminish outward to <0.3 mm/yr toward the flanking basalt and sedimentary rocks. No active structures or faults are known in the lowland regions of the West Fork Satsop, although Quaternary glacial drift covers much of the region. Pleistocene valley glaciers sourced in the Olympics left outwash terraces in the Satsop basin, whose channels have both bedrock- and alluvium-floored reaches. Gaging stations on the main stem Satsop River recorded the 70 yr flood of record during the extreme winter rainfalls of 1996–1997. Old-growth Douglas fir and cedar forest covered the land prior to historic clear-cutting in the first half of the twentieth century. Montgomery et al. (1996) argued that many channels in the basin were alluvial prior to removal of logjams and large wood during logging.

We chose three bedrock reaches of the W.F. Satsop and one on a tributary called Black Creek to monitor bedrock lowering. The upstream site on the W.F. Satsop (Fig. 4A), is several hundred meters downstream of Eocene Crescent basalts in a mixed alluvial and bedrock reach cut in poorly cemented, thin-bedded sandstone and siltstones of the unnamed Eocene unit (Fig. 2) that strikes across the stream and dips southward. A narrow bedrock bench above the channel thalweg is exposed on both banks during base flow, and a V-shaped low-flow channel is cut ~1 m deep into it. We found cut wood fragments in deposits on a bedrock surface 1.2 m above the bench, indicating historic abandonment of an ~100-m-wide surface now covered by 1 m or more of alluvium and remnant logjams. These deposits indicate that this reach was alluvial, at least during early post-European contact years and probably until logging in the 1940s to 1950s. Approximately 500 m downstream on the Lower W.F. Satsop, we chose two sites near each other with exposed siltstone and mudstone of the Lincoln Creek Formation. Upstream and downstream of these sites are alluvial reaches with strath terraces of varying elevation and low flow depths of ~0.7 m. Black Creek (Fig. 4B) cuts poorly cemented upper Miocene sandstones of the Montesano Formation (Tabor and Cady, 1978). When surveyed in 1995, the channel had little alluvial cover except for where forced alluvial reaches were impounded by logjams (Montgomery et al., 1996). Low flow is <0.1 m deep, although we found trimlines from a 1996–1997 dam-break flood of ~1 m depth, which removed many of the forced alluvial reaches (Montgomery et al., 2003).

In addition to the W.F. Satsop and Black Creek, we selected the nearby basins of the Middle Fork Satsop River and the Canyon River for long-profile analysis. The profiles of the Middle and W.F. Satsop and Canyon River, head in basalt before crossing sandstone and siltstones of the unnamed Eocene sedimentary rocks at the mountain front and the Lincoln Creek and Montesano Formations downstream.

Washington Cascades

The W.F. Teanaway (West Fork of the Teanaway River) heads in glaciated Eocene sandstones of the Swauk Formation near the crest of the Washington Cascades and flows downstream through middle Eocene basaltic, andesitic, and rhyolitic rocks of the Teanaway Formation (Tabor et al., 2000). High-relief steep lands associated with these rocks cease at a lithologic boundary with overlying Eocene micaceous sandstones and siltstones of the Roslyn Formation, into which is cut a wide, low-relief valley. Miocene Columbia River basalt flows in the region are warped up to the west toward the Cascade crest, as is a 1 Ma intracanyon andesite on the Tieton River to the south that has been incised at an average rate of ~0.1 mm/yr at its upstream end (Donald Swanson, Hawaiian Volcano Observatory, Hawaii, 1996, personal commun.). This local river-incision rate is less than the estimates of 0.15–0.25 mm/yr for regional long-term exhumation rates east of the Cascade crest (Reiners et al., 2002). The basin of the W.F. Teanaway is typically snow covered in winter and is the site of a spring snowmelt peak in May.

Roslyn Formation sandstones are nearly continuously exposed along the lower ~3 km of the W.F. Teanaway, and in patches in the ~9 km upstream. These medium- to fine-grained, white, micaceous, lithofeldspathic sandstones have weathering features like those shown in Figures 2–3. Above base flow, much of the bedrock surface consists of weathered flakes ~0.01–0.1 m thick, some of which expand upward and form "tents" during the dry season. In the study area, the river has incised 1–2 m into a low-relief bedrock surface and has a parabolic channel cross section with little sediment cover. However, gravel in these reaches was abundant enough during 1936 field surveys (Federal Bureau of Fisheries) that ~65% of the streambed in the lower 11 km of the Teanaway was judged to be suitable for fish spawning (McIntosh et al., 1995). Descriptions and a photograph of the adjacent Middle Fork (Teanaway River) at the beginning of the twentieth century (Russell, 1898) record abundant in-channel wood, common in Pacific Northwest rivers prior to logging and stream cleaning (e.g., Sedell and Luchessa, 1981; Collins et al., 2002). In the Teanaway, timber companies began such activities early in the twentieth century (Shideler, 1986), transporting logs by river drives (1902–1916) and railroads (1917–1930). Disappearance of alluvium along much of the W.F. Teanaway, and 1–2 m of incision into the bedrock occurred sometime in this century, likely as a result of these activities. In addition to long-profile analysis of the main stem, we installed three cross sections of erosion pins from kilometer 2.0 (measured from the confluence with the Middle Fork, Teanaway River) to kilometer 2.6. Within the low-flow channel, bed surfaces frequently have ~0.1–1.0-m-wide flutes.

Oregon Cascades

Walker Creek (Fig. 4C) dissects Oligocene–Miocene (35–25 Ma) volcanic and volcaniclastic rocks (Sherrod and Smith, 2000) in foothills of the Western Oregon Cascades near Eugene, an area with northwest-trending high-angle faults that have been active during the Neogene. Reservoir sedimentation surveys of Dorena Lake (Dendy and Champion, 1978), downstream of Walker Creek, and nearby Cottage Lake, indicate sediment yields that are equivalent to lowering rates of 0.03 and 0.05 mm/yr over a period of 5–10 yr, under the assumption of commonly reported sediment bulk-density values of 1120 kg/m^3 (Dendy and Champion, 1978). Locally, Walker Creek cuts lahars in its lower reaches, and rhyolite ash flows and dacites in its upper reaches. The lahars are strongly indurated with both rounded and angular lithic fragments in a cemented, clay-rich matrix. Where exposed in the stream channel, bedrock surfaces have folia and tented folia (Fig. 3B) that indicate the potential for rapid erosion. Roads were built across a headwater portion of Walker basin to clear-cut the forest. A road-related landslide during the winter of 1996–1997 dammed the main stem, resulting in a dam-break flood that reached depths of 5 m and left ~650 m of bedrock thalweg exposed over 1300 m from the dam-break to the downstream-most bedrock exposure. Starting at this location, we spaced four cross-sections at ~325 m intervals upstream along the flood path. The lower three are in indurated lahar deposits, and the uppermost cross section is in an indurated rhyolite ash flow, which has strong secondary silica cement. Cutbanks and a few preserved mid-channel deposits at the lower cross sections along Walker Creek are composed of matrix-supported diamictons, which—because glaciation did not reach these lower elevations—are likely old debris-flow deposits. We chose profiles from Walker Creek and its main stem, Sharps Creek, to examine area vs. slope data. Sharps Creek traverses indurated dacite pyroclastic flows and lahar deposits in its headwaters and basalt flows in the last several hundred meters above a major tributary junction upstream of Dorena Lake.

Oregon Coast Range

Landslides during 1996–1997 El Niño storms initiated debris flows throughout the Oregon Coast Range (e.g., Hofmeister, 2000), many of which scoured sediment from valley floors and exposed carbonate-cemented sandstones and siltstones of the Eocene Tyee Formation. We used ground reconnaissance to locate debris-flow sites in Sullivan Creek basin, near Coos Bay. Erosion rates in this part of the central Oregon Coast Range are thought to be between 0.1 and 0.2 mm/yr on the basis of strath-terrace ages (Personious, 1995), sediment yield (Reneau and Dietrich, 1991), and cosmogenic radionuclides (Heimsath et al., 2001). Here and in the nearby Marlow Creek basin, we walked debris-flow runouts (dotted lines in Fig. 5) to map the occurrence and style of bedrock lowering from debris flows. We observed folia and tented folia (Fig. 3A) along these runouts. Although difficult to quantify systematically, we found that debris flows had removed bedrock as (1) grooves and lineations at the scale of the component rock grains, and as (2) fracture-bounded blocks one to several centimeters thick, corresponding to folia. We installed 20 cross sections of 221 erosion pins (placed at 0.25 m spacing) along the upper 350 m of bedrock exposed and eroded by a 1997 debris flow in an unnamed tributary of Sullivan Creek. Individual dots in Figure 5 approximate cross section spacing. An additional 142 pins were installed along 195 and 240 m of two debris-flow runouts in Marlow Creek, at a similar frequency. We also installed two cross sections of erosion pins on the main-stem Sullivan Creek, which has year-round base flow, well-defined fluvial banks, and pool-riffle reaches locally. Matrix-supported deposits interbedded with fluvial deposits indicate that debris flows also occurred along this reach. We chose long profiles (1) for the unnamed tributary creek to illustrate the curved area vs. slope form that we commonly observe in valleys scoured by debris flows (Stock and Dietrich, 2003), and (2) for Sullivan Creek, which has a short reach below a large knickpoint.

California Coast Range

The S.F. Eel (South Fork of the Eel River) cuts Cretaceous marine sandstones of the Franciscan Formation in the northern California

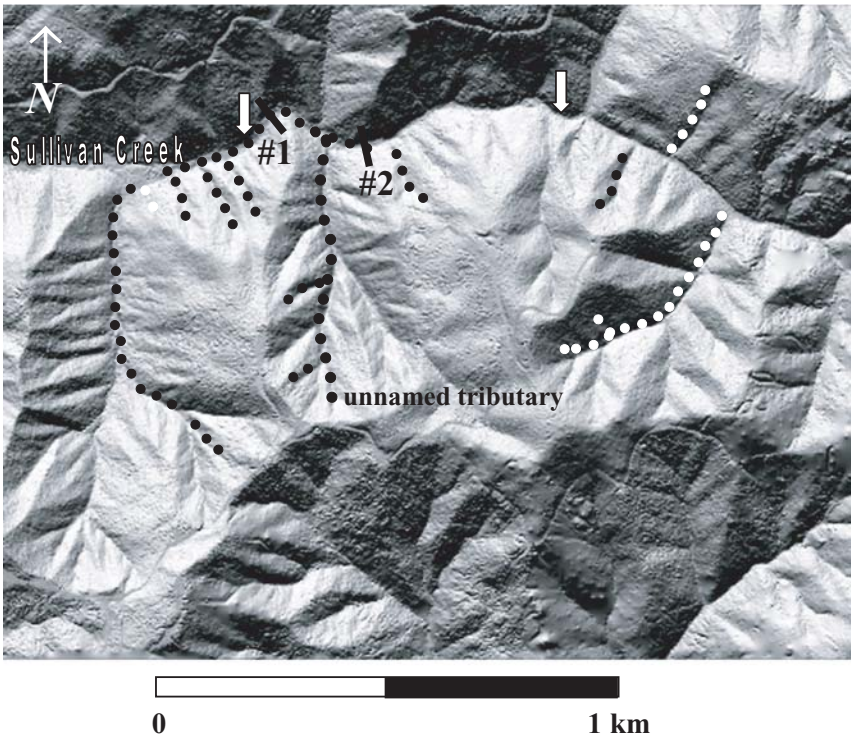

Figure 5. Hill-shaded laser altimetry (~2 m horizontal resolution) from Oregon at Coos Bay. Dotted lines indicate 1996–1997 debris flows, as mapped in the field. Arrows bracket knickpoint on Sullivan Creek. Numbers refer to erosion-pin cross sections on Sullivan. Pin cross sections on the unnamed tributary to Sullivan Creek are too numerous to show, but occur approximately at every dot.

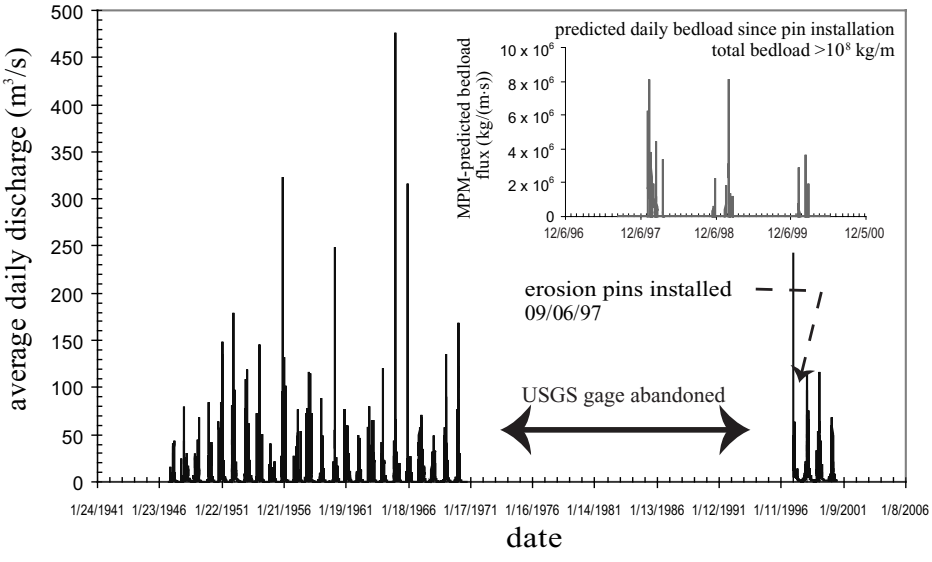

Figure 6. Average daily discharge for S.F. Eel at Branscomb gage (#11475500). Values from 1997 to 2000 are from a stage recorder operated by U.C. Angelo Reserve staff. Inset shows an illustrative calculation of bed-load transport capacity past the erosion-pin site for the period of stage record; the calculation used the Meyer-Peter and Mueller (MPM) bed-load equation as found in Julien (1998: equation 9.3a). Excess shear stress calculated by using stage data with τ^*_c equal to 0.047 and grain-size and slope data in Table 1. These values are two orders of magnitude larger than regional values from sediment-yield estimates of bed load, consistent with excess transport capacity at this bedrock reach.

Coast Range. Knickpoints in the South Fork's longitudinal profile and strath terraces on the main stem and tributaries (Seidl and Dietrich, 1992) record locally transient river-incision rates. Canyon walls confine the river along much of its course, leading to floods of considerable depth. For instance, trimlines from the 1964 flood of record indicate flow depths of ~4 m at a water-surface slope of ~0.004 near the Elder Creek confluence. Average annual sediment loads estimated at 1700 t/km^2 yr for the entire Eel basin (Milliman and Syvitski, 1992) are equivalent to basin-wide lowering rates of 0.6 mm/yr, values similar to those of 0.5 mm/yr estimated by inland projection of marine-terrace rock-uplift rates from Merrits and Vincent (1989). This value for basin-wide sediment yield likely overestimates long-term lowering rates in the headwaters of the S.F. Eel because it includes substantial increases due to anthropogenic effects (e.g., Sommerfield et al., 2002). Consequently, long-term lowering rates are likely to be <0.6 mm/yr. We installed erosion pins on a largely bedrock cross section (Fig. 4D) at the location of a USGS (U.S. Geological Survey) gage whose daily record was discontinued in 1970 (USGS gage #11475500). This is the only site near a gaging station. A partial stage record is available for the first several years after pin installation (Fig. 6); however, the stage data are unreliable after 1999 (Tracy Allen, University of California Angelo Reserve, 2002, personal commun.). A strath terrace 2.3 m above the thalweg on the left bank records past river incision into the bedrock. We collected width and grain-size data in alluvial reaches upstream of this bedrock-dominated knickpoint area in addition to area vs. slope analysis.

Western Foothills, Taiwan

In September 1999, the Chelong-Pu thrust fault ruptured along ~200 km of eastern Taiwan during the Chi-Chi earthquake (e.g., Kao and Chen, 2000; Rubin et al., 2001). Coseismic displacement was largest along the north end of the fault at the Tachia River and declined to <1 m south of Nantou (e.g., Rubin et al., 2001). A narrow (<1 km wide) belt of Chinshui Shale crops out along much of the Chelong-Pu fault (Ho and Chen, 2000) and is locally exposed at waterfalls formed by the 1999 rupture. The Western Foothills rise to the east of the Chelong-Pu fault, an out-of-sequence thrust (Kao and Chen, 2000). This region is composed of eastward-dipping monoclines of sandstone, siltstone, and shale of the Pliocene–Pleistocene Cholan Formation and, farther eastward, the Toukoshan Formation, a Pleistocene equivalent with similar lithologies. These units are in thrust contact with older

Miocene sandstone, siltstone, and shale farther east, which make up the rest of the Western Foothills. The boundary of these foothills with the high-relief (e.g., >1 km) region of the Central Range coincides with Eocene to Oligocene metasedimentary rocks including shale, slate, argillite, phyllite, arkoses, and quartzites that make up much of the Central Range. Strath terraces occur in most of the larger rivers draining the Western Foothills and are widely interpreted to be of tectonic or climatic origin (e.g., Chen and Liu, 1991; Sung et al., 1995, 1997; Hsieh and Kneupfer, 2001). Apatite fission-track thermochronology referenced in Liu et al. (2001) indicates exhumation rates of ~1 mm/yr over the past several million years in the Western Foothills. Suspended loads reported for the Tachia River (Li, 1976) are equivalent to basin-wide lowering rates from 0.12 mm/yr in the Central Range part of the catchment to 0.10 mm/yr near the coast; because of the influence of upstream dams, these are likely underestimates of lowering. Rates from nearby catchments draining the Central Range or Western Foothills range up to 1.1 mm/yr. Yearly typhoons can drop up to 1 m of water per day in the Western Foothills (e.g., Chang and Slaymaker, 2002).

In an effort to document the response of these knickpoints over the year following the earthquake, we surveyed river-crossing scarps in the northern sections that included four sites where the rupture exposed bedrock of the Chinshui Shale (named Tachia, Tali, Tsao-Hu, and Chang-Ping on 1:50,000 geologic maps). Sites were selected in January 2000 for their range of drainage areas and minimal modification by postearthquake engineering. At the northern edge of coseismic rupture, we installed erosion pins at the Tachia River, which drains part of the Central Range of Taiwan, including all of the lithologies summarized above. In the other southern basins, Chinshui Shale at the rupture is followed several hundred meters upstream by Cholan Formation, and by Toukoshan Formation (see Stock, 2004, for locations). The smaller basins south of Tachia are cut back into a monocline of eastward-dipping Cholan and Toukoshan units that forms the Eastern Foothills here. The Chang-Ping basin, near the city of Nantou, also has outcrops of older Miocene sandstone and shale in its headwaters.

During our initial visit in January 2000, we noticed that siltstones and mudstones of the Chinshui Shale weathered rapidly when exposed above base flow, generating a 60–120-mm-deep zone of strongly fractured rock. In the southern basins, strath terraces are inset within modern concrete levee walls that bound one or both banks of the channel. At Tsao-Hu, hydraulic structures have collapsed over the strath, indicating strath formation after the channel was modified by engineers. Here we installed pins in a dipping bedrock ramp created by co-seismic folding that formed the only exposed bedrock in the reach. At the other three sites we installed erosion pins many meters upstream of the fault scarp. We surveyed strath terraces and examined fill on them for historical artifacts. Base flow at the Tali, Tsao-Hu, and Chang-Ping sites is confined to the channel thalweg, exposing wide adjacent bedrock surfaces to wetting and drying whose results we monitored with erosion pins. We collected area vs. slope data for these sites by using 1:5000 and 1:50,000 scale topographic maps.

METHODS

At each study site we chose a reach of uniform bedrock where we observed folia (Fig. 3) or pervasive weathering features (Fig. 2). We installed a cross-section line of erosion pins to monitor short-term production rates of both folia and pervasive weathering features. At each cross section, we spaced erosion pins at equal intervals, from 0.25 m for narrow channels to 1 m for wide channels (see Table 1 for details). At a few sites (Satsop in Washington and Tachia in Taiwan), coverage ends where base-flow depth exceeds the drill-bit length of 100 mm. At the Olympic and Teanaway sites, additional erosion pins were installed on cross sections 1 m upstream and downstream off the main line with 1 m spacing to estimate spatial variations in lowering rate. In Taiwan and on the Lower W.F. Satsop, shales were already weathered enough to emplace long nails into the bedrock with a sledgehammer. Elsewhere, we predrilled holes by using a Bosch rotary-impact drill and installed erosion pins of slightly larger diameter by using a sledgehammer. At sites with pervasive weathering features (Taiwan, Satsop, Black Creek), we used 125–160-mm-long nails as erosion pins because we anticipated large amounts of lowering. At sites with only folia, we used 60-mm-long hollow-wall anchors with drive points because they have brackets that expand to grip the hole upon emplacement. All erosion pins had their heads flush with the local surface; the microtopography of this surface limits measurement precision to ±1 mm. To evaluate whether installation of the erosion pins affected the measured local erosion rate: (1) at Upper W.F. Satsop, we left half of the cross section as holes of known depth in order to evaluate the influence of driving nails into the rock; and (2) we surveyed points between the nails to evaluate the influence of drilling on lowering. We also surveyed the elevation of the top of each erosion pin and referenced it to benchmarks driven into bedrock on the bank. We returned to the Olympic and the S.F. Eel sites to remeasure erosion-pin cross sections two to three times, as indicated by alternate values for lowering rates in Table 2. Erosion rates at other sites were estimated from one return measurement.

At sites with folia, we measured the thicknesses of 100 samples by random walk within a cross section that included both wet and dry bedrock several meters up- and downstream of the erosion-pin cross section. We used a pencil tip to choose a sample, and detached it to measure the maximum surface-normal thickness. At a few sites, we found <100 samples near the cross section during our first visit (e.g., Walker Creek). At the Tsao-Hu site in Taiwan we estimated the thickness of the weathered zone by excavation of multiple folia.

At each cross section, we measured the slope of the bedrock channel floor by using tape and hand-level over a length of 7–10 multiples of channel width, and we measured drainage area from contour maps. We estimated channel width by using recent flow-line indicators, and measured valley width as the distance between steep valley walls. At U.S. sites we estimated base flow by using average velocity and cross-section area of inundation at the time of our visits (usually during dry summer months). We crudely estimated the size distribution of bed load that crossed our sites when we returned to measure erosion-pin cross sections by choosing active bar tops for Wolman method point counts. This approach would tend to overestimate the coarse fraction of bed load if armoring occurred. We also collected carbon samples for ^{14}C dates from detrital charcoal in basal fluvial deposits on strath terraces near Olympics sites.

To construct area vs. slope plots, we measured drainage area and slope by hand from topographic maps at 1:24,000 (U.S.) or 1:50,000 (Taiwan) scale by using techniques described in Stock and Dietrich (2003). For long profiles all in a single lithology (e.g., S.F. Eel and Sharps Creek), we separated fluvial log–log-linear data from curved data by using a threshold curvature technique described fully in Stock and Dietrich (2003). For profiles with mixed lithologies (Satsop, Teanaway, Taiwan rivers), we separated area vs. slope data corresponding to lithologies in which we had erosion-pin sites. We then estimated profile concavity by regressing the log–log-linear parts in both cases with a power law. For sites with laser altimetry in Sullivan Creek, we extracted the valley network by using threshold drainage areas of 1000 m^2, based on field observations of channel-head location (Montgomery and Dietrich, 1992). We used a maximum-fall algorithm for slope with a forward difference of two grid cells, extracted the

TABLE 2. EROSION DATA FOR SITES WITH EROSION PINS

Region stream	Anthropogenic activity	Folia mode (mm)	Mean (mm)	St dev	*N*	Pin length (mm)	*n*	Pin spacing (m)	Median pin lowering (mm/yr)	Mean (mm/yr)	Meas. time (yr)	Historic (mm/yr)	Strath (mm/yr)	Geologic (mm/yr)	Bed load flux (× 10^3 kg/(m·yr))
Olympics, Washington															
West Fork, Satsop	logjam removal	-	-	-	-	120–160	37/49	0.50	41/>130	44/>114	1/1	20–30	-	< 0.3	440
Lower West Fork (1)	"	-	-	-	-	~200	14	0.25	137	39	1.6	-	-	"	600
Lower West Fork (2)	"	-	-	-	-	160	28	0.5	>160	>160	1	-	-	"	600
Black Creek	"	10–15	9.3	2.0	210	120–160	56/56	0.50	9/62	14/61	1/1	-	0.3–0.7	"	65
Cascades, Washington															
Teanaway (1)	"	NC	NC	NC	NC	76	62	0.50–1.0	18.3	>28	1	-	-	~0.05–0.10	53–110
Teanaway (2)	"	NC	NC	NC	NC	76	62	0.50–1.0	3.7	>6.5	1	-	-	"	90–180
Teanaway (3)	"	NC	NC	NC	NC	76	40	0.50–1.0	3.9	>7.4	1	-	-	"	61–120
Cascades, Oregon															
Walker (1)	dam-break flood	5–10/10–15	10.2/12.3	1.83/1.65	49/100	56	24	0.50	0 (0–0.5)	1.1	4	-	-	0.03–0.05?	3–5
Walker (2)	from road-related	NC	NC	NC	NC	56	22	0.25	0	0.03	4	-	-	"	5–8
Walker (3)	landslide	5–10/10–15	8.07/10.7	1.93/1.72	10/100	56	23	0.25	0	0.54	4	-	-	"	5–8
Walker (4)	"	-	-	-	-	56	20	0.25	0	0	4	-	-	"	3–5
Oregon Coast Range															
Sullivan (1)	debris flows from	-	-	-	-	56	16	0.50	0	0	4.1	-	-	0.07–0.10	5–8
Sullivan (2)	clear-cut	15–20	15.5	1.6	31	56	31	0.25–0.50	0	0.13	4.1	-	-	"	5–8
Sullivan tributary	"	7–8	8.8	3.3	9855	56	221	0.25	0	0	4.1	-	-	"	
Marlow Creek trib.1	debris flows from	4–5	8.9	7.5	1014	56	80	0.25	0	0	4.1	-	-	"	
Marlow Creek trib.2	altered forest	4–5	6.9	6.8	705	56	62	0.25	0	0	4.1	-	-	"	
California Coast Range															
South Fork, Eel	"	-	-	-	-	56	33	0.50	0.6/0.75	1.7/3.9	3.9	-	-	~0.5–0.6	150–750
Taiwan, Western Foothills															
Tachia	dam	NC	NC	NC	NC	125	56	0.50	>125	>125	1	-	-	0.1–1.0	290–2900
Tali	levee	NC	NC	NC	NC	125	40	0.50	>125	>125	1	-	-	"	34–340
Tsao-Hu	"	45	42.5	1.4	45	125	14	0.50	>125	>125	1	-	-	"	18–180
Chang-Ping	"	NC	NC	NC	NC	125	20	0.50	>125	>125	1	26	-	"	110–1100

Note: NC—not collected; trib.—tributary; back slashes separate reoccupations of sites; folia data collected at reoccupation, except for Walker Creek where values for installation are shown first; historical lowering rates estimated from straths with cultural artifacts in their fill; strath lowering rates estimated from radiocarbon-dated samples in their fill, and geologic estimates from sediment yield, cosmogenic radionuclides, or mineral cooling ages (see text); bedload flux per unit width estimated using geologic lowering ranges and assuming bedload is 10% of total load.

profile data, and averaged it to 10 m to smooth the effects of cliffs in thick-bedded sandstones. Debris-flow runouts for Marlow Creek in the Oregon Coast Range were so short that USGS topographic maps had only a few points for area vs. slope plots, and are therefore omitted.

To estimate rock-mechanical properties associated with rapid lowering rates, we took rock samples from all of the field sites and maintained field moisture conditions by keeping the samples saturated. For W.F. Satsop, Sullivan Creek, and S.F. Eel, we successfully removed large blocks of the rock exposed at the cross sections. We cut these into 200-mm-diameter discs for abrasion-mill tests of rock erodibility to bed load following the methodology of Sklar and Dietrich (2001). For other sites, we either could not carry a large enough sample out (Black Creek, Teanaway), or samples proved to be too fractured to cut into large discs (Walker Creek and the Taiwan sites). Because Sklar and Dietrich (2001) have demonstrated that tensile strength is a relevant measure of rock resistance to bed load erosion, we measured the tensile strength of the remaining samples by using the Brazilian tension splitting test (e.g., Vutukuri et al., 1974). To estimate the resistance of the rock to weathering by periodic wetting and drying, we submerged samples in water overnight and dried them at 40 °C in an oven during the day. Following the methodology outlined in ASTM (1997), we weighed the fraction of the original block that shed during each cycle as a measure of the rate of breakdown. We chose a lower oven temperature than that recommended in ASTM (60–70 °C) in order to approximate environmental conditions at field sites.

RESULTS

Erosion Pins

Erosion pins recorded bedrock lowering of millimeters to centimeters per year at each study site (Fig. 7; Table 2). Mean lowering rates at most sites are much larger (1–3 orders of magnitude) than long-term erosion-rate estimates (Fig. 8; Table 2). Figure 7 illustrates the

Figure 7. One to several years of bedrock lowering indicated by erosion pins in (A) W.F. Satsop, (B) Black Creek, (C) Walker Creek (site 1), and (D) S.F. Eel. See Table 2 for details. Note that pin protrusion above the surface indicates pervasive lowering, not localized scour or damage from installation. Lowering in the Satsop and Eel is by detachment of centimeter-sized weathered fragments during high flow. Lowering at Black and Walker Creeks is by folia generation and removal during high flow.

fact that bedrock lowering is not confined to pin sites, as it would be if pin installation strongly influenced lowering rate. Hand-level resurveys at W.F. Satsop, for instance, also indicate the same magnitude of lowering away from pins. By contrast, steep valleys scoured by debris flows before pin installation had numerous folia, but no lowering occurred in any of the 363 erosion-pin sites at the unnamed tributary of Sullivan Creek or in the Marlow tributaries between 1997 and 2001 (Fig. 9; Table 2). Repeat photography at cross sections indicated gradual infilling (Fig. 9B) over scoured bedrock by hillslope sediment and vegetation and no new folia production or transport.

Figures 10–11 illustrate another contrast, between patchy folia production (Walker and Sullivan Creeks) and pervasive bedrock weathering above base flow (Satsop, Black Creek, Teanaway, Eel, Taiwan). Localized folia production in Walker and Sullivan Creeks leads to patchy removal of parts of the channel bed. At sites with pervasive weathering, erosion pins record bedrock-lowering rates as fast as hundreds of millimeters per year, consistent with seasonal production and removal of several folia depths (Table 2). Above base flow, lowering is continuous across the section and occurs by entrainment of weathered product during seasonal high flows and perhaps bed load abrasion during peak flows (and dam-break floods in the case of Black Creek). Lowering rates decrease below the base-flow waterline, consistent with reduction in weathering rate. Nonzero lowering rates in thalwegs record bed-load abrasion rather than plucking because of the continuous pattern of lowering. For instance, the S.F. Eel (Fig. 10), had relatively continuous lowering at several millimeters per year across the erosion-pin cross section, with an abrupt drop at the base-flow boundary. Below water level, the bedrock surface is smooth and devoid of open fractures, and erosion pins are polished. Bed load flux estimates at S.F. Eel determined from stage data with the Meyer-Peter and Muller equation (Fig. 6) are two orders of magnitude larger than the estimated average annual bed load fluxes (Table 2), consistent with excess transport capacity at this site. Historic peak discharges 2–5 times as large as those that occurred during the erosion-pin monitoring (Fig. 6) suggest that decadal lowering rates might be substantially larger.

Mean and median lowering rates exceed 100 mm/yr over 7 yr of pin measurements at W.F. Satsop, 100 mm/yr at Lower W.F. Satsop site 1 for 1 yr, and 50 mm/yr at Lower W.F. Satsop, site 2 for 2 yr. A number of pins from W.F. Satsop, were entirely removed, so we can only constrain minimum lowering rates of 120 mm to 160 mm, depending on pin length. Median rates from 2 yr at W.F. Satsop, are 41 and >130 mm/yr, and those at Black Creek are 9 and 62 mm/yr. One-year median lowering from sites 1 and 2 on the Satsop are 137 mm and >160 mm, respectively. At Satsop, these rates represent lowering of a platform above the thalweg, whereas Black Creek data represent thalweg lowering. There was an increase in incision rate at both sites in 1996–1997, coincident with high discharges that year. In particular, large increases in the lowering rate at Black Creek coincide with a dam-break flood in winter 1996. We observed smaller lowering rates below base flow than above it during the first year at the W.F. Satsop and Black Creek. Median lowering on Black Creek is four times greater in the zone above base flow (16 mm) than below it (4 mm). At W.F. Satsop, lowering rates also decline sharply from 70 mm above observed base flow to <1 mm below it.

Revisits to W.F. Satsop and Black Creek during winter high flows in 2001 indicated that high rates of lowering continued. Flow was too deep at the time of measurement to examine whether bedrock had remnant holes or had lowered entirely past the original pin. Flood marks at W.F. Satsop indicated recent flows of ~1 m depth across the platform with the pins, and some quantity of bed-load transport across it was indicated by isolated deposition of cobbles. At Black Creek, flow was too deep to measure lowering, although we could tell that several centimeters of erosion had occurred between 1997 and 2001 because some pins were entirely missing.

Teanaway sites had mean lowering rates of >6–28 mm/yr, >60 times the largest estimate for long-term lowering rate (Table 2). Many pins were removed entirely, although a few located high on cross section 3 showed no lowering (Fig. 10). Sullivan cross section 2 (not shown) lies entirely below base flow and has no folia or detectable lowering (Table 2). Sullivan cross section 1 and Walker cross sections 1–3 had a few sporadic folia and associated lowering in areas of shallow base flow. Pins below base flow were algae-covered and unabraded. Sites without folia did not lower and were either entirely below base flow (Sullivan site 2) or in strongly cemented rocks like the silicified ash flow of Walker cross section 4. In Walker Creek, resurveys indicated that minor deposition occurred along the path of the dam-break flood since 1997, and a few plate-like folia <1 m downstream from their source also indicate only minor sediment transport.

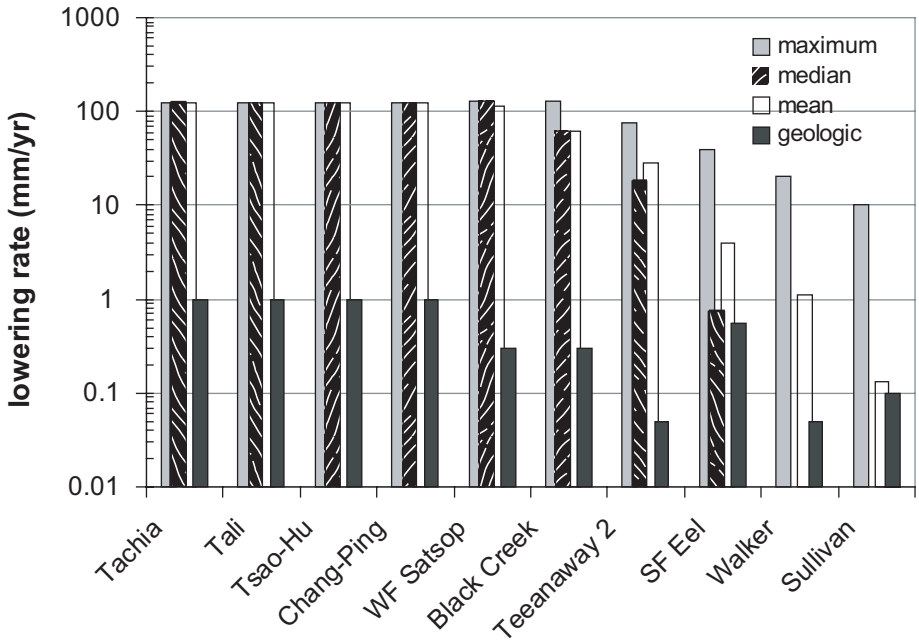

Figure 8. A comparison of maximum estimates for long-term erosion rates with short-term erosion-pin rates for rivers in Taiwan (Tachia, Tali, Tsao-Hu, and Chang-Ping), Washington (W.F. Satsop, Black Creek, Teanaway 2), California (S.F. Eel) and Oregon (Sullivan 1). Short-term lowering rates on Taiwanese and Washington rivers are minimums because erosion pins were entirely removed. Except for sites in debris-flow runout zones in Oregon, short-term averaged rates exceed long-term rates. In all cases, maximum observed erosion rates exceed long-term rates.

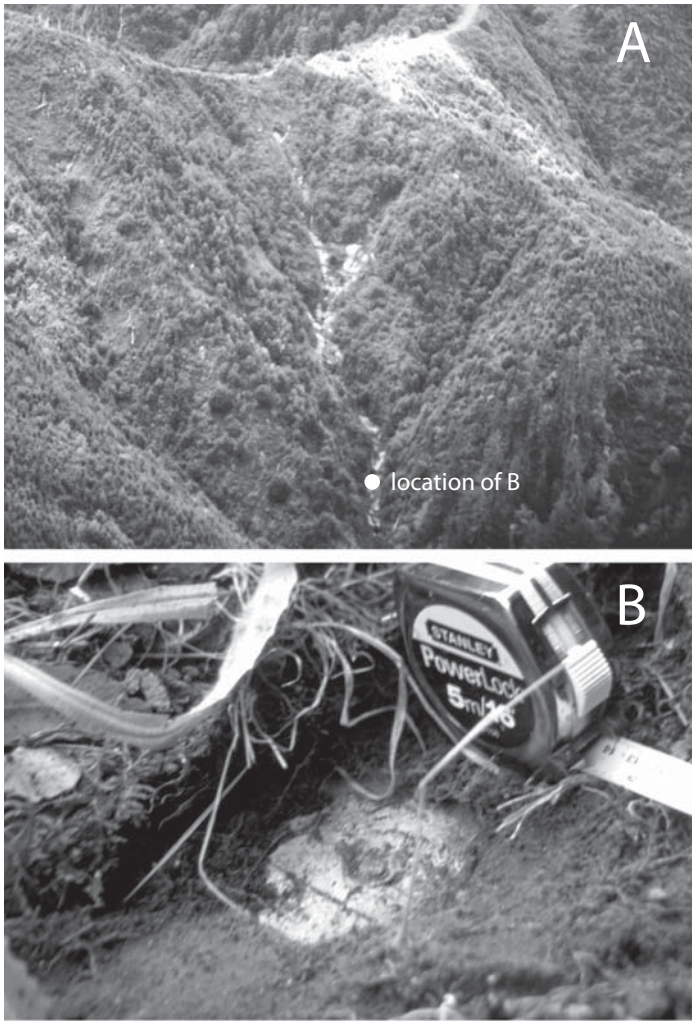

Figure 9. (A) Runout path of Sullivan Creek unnamed tributary (see Fig. 5) debris flow (light areas of bedrock, starting at top middle) shortly after failure occurred in winter 1996. Note the widely exposed bedrock, which was lowered along much of the runout path during the debris flow. (B) Pin buried with colluvium by 2001. The fact that most of the >200 erosion pins emplaced shortly after the debris flow were buried by 2001 indicates no bedrock erosion in the intervening years.

High rates of bedrock lowering occurred at the Taiwan sites (Table 2; Fig. 12). In 1 yr, rebar benchmarks and all erosion pins were removed at all sites except Tachia, indicating lowering rates in excess of 125 mm/yr. At Tachia, one erosion pin remained (~47 m on cross section), allowing us to reconstruct an approximate cross section for a part of the right bank that we surveyed in 2000 (Fig. 12A). The differences between the initial and resurveyed cross section indicate over 2 m of lowering in places, accomplished by a combination of weathering and bed-load abrasion. At Tsao-Hu and Chang-Ping, the 1999 fault scarp was eliminated as a discrete feature over the course of a year, so it is unclear whether lowering rates at these sites were influenced by scarp retreat or not. At Tali the fault scarp remains identifiable, so that lowering around pins was not a result of scarp retreat.

Folia

The magnitude of lowering in Figures 10–11 is consistent with erosion of one to several folia, which are an average of between 9 and 15 mm thick (Fig. 13). For instance, lowering rates at Black Creek are compatible with the generation and removal of an average folia thickness the first year, and several folia layers in the second year. Larger values for Taiwan shales record formation of thick weathering zones rather than discrete folia. Most thickness distributions are log normal as measured by normal quantile tests. The seasonal production of these features is pervasive in some localities (Satsop, Black, Eel, Taiwan) and patchy in others (Walker, Sullivan). The number of folia increased with time at Walker Creek, as shown by the larger number of folia measured at reoccupation in 2001 (Fig. 13) and by repeat photography that illustrated the conversion of large sections of formerly intact rock to folia. Preservation of folia is likely due in part to low flow and sediment-transport rates, as indicated by maximum stage indicators less than several decimeters over the monitoring period (D_{max} in Table 1); recently transported bed load is also small (site D_{50} in Table 1 is 5 mm).

Strath Terraces

Cultural artifacts deposited on strath terraces in Washington and Taiwan indicate historic abandonment. At W.F. Satsop, the flood-plain surface consists of a mosaic of low-elevation channelways now overgrown with 40–50-yr-old alder and higher surfaces upon which cedar and fir grow and where old-growth stumps occur on local high spots between abandoned channelways. We found cut wood within the alluvium on the strath, confirming that the terrace surface was a historically active depositional surface. This inference implies an average lowering rate of 1.2 m per 40–50 yr (i.e., 24–30 mm/yr). Because logging began here in the 1940s (N. Phil Peterson, Simpson Timber Co., Shelton, Washington, 2000, personal commun.), this feature indicates sustained bedrock-lowering rates of >20 mm/yr, depending on exactly when incision began. Measured rates of incision from erosion pins (>44 mm/yr) are sufficient to have converted the historical flood plain into an abandoned strath terrace capped by gravels since the flood plain was logged. Downstream of Lower W.F. Satsop, site 2, alluvium on 0.4- and 5-m-high straths contains detrital charcoal dated to 1290 (±100) and 7400 ± 50 yr B.P., respectively. Longer-term lowering rates from these strath terraces of 0.3–0.7 mm/yr are consistent with apatite fission-track exhumation rates from Brandon et al. (1998). At Teanaway, the ages of strath terraces inset ~1–2 m above the current channel are likely historic on the basis of riparian tree ages.

In Taiwan, lowering rates in excess of hundreds of millimeters per year are recorded by incision below the level of historic engineering structures. Figures 12B and 12C show cross sections and long profiles for a reach downstream of a small retaining dam, where bedrock

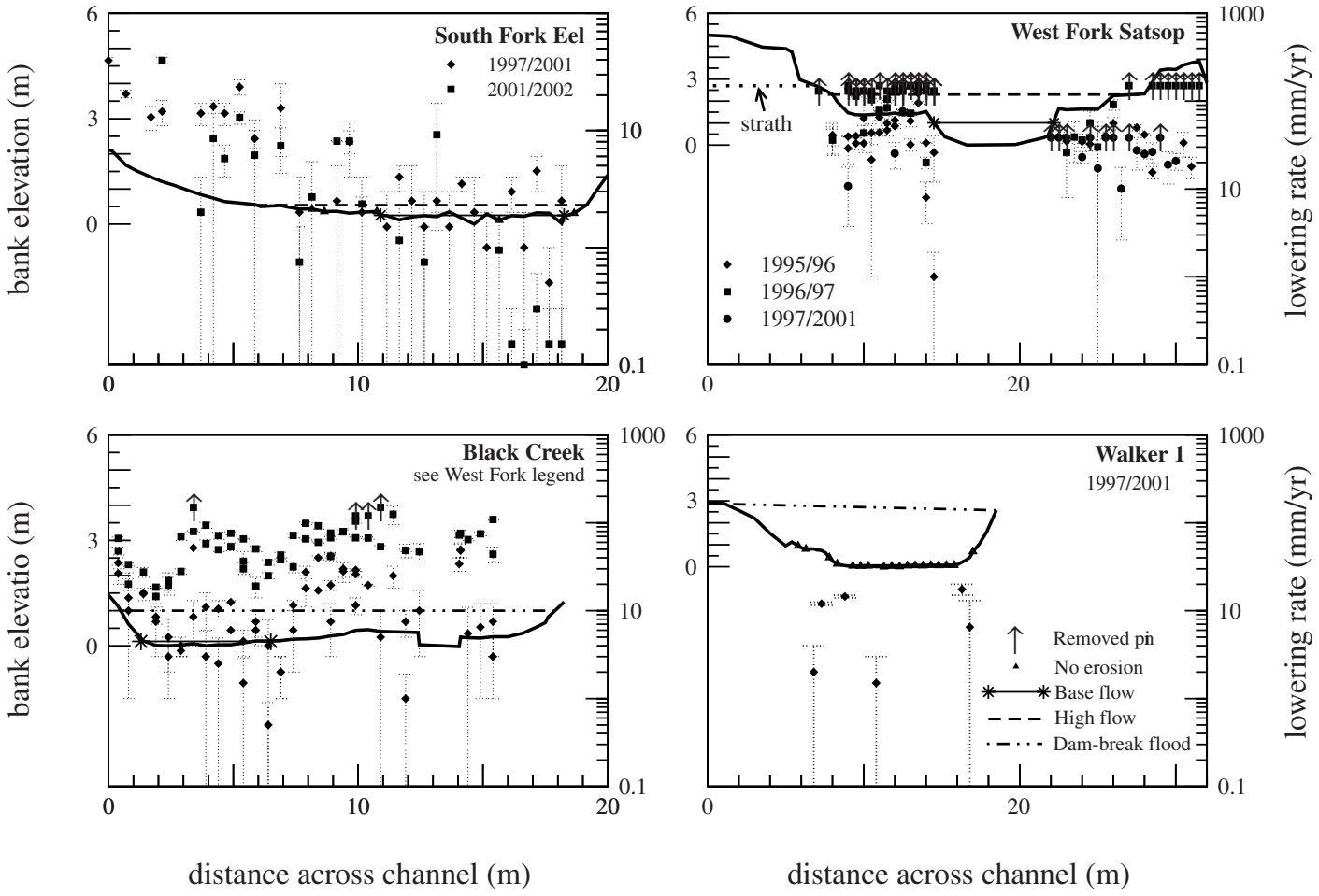

Figure 10. Yearly lowering rates from erosion pins (right y-axis), and cross sections (left y-axis) for S.F. Eel, California; W.F. Satsop, Black Creek, Olympic Mountains, Washington; and Walker Creek 1, Oregon Cascades. See Table 1 for site details. Dashed vertical lines through symbols indicate maximum and minimum lowering observed around individual pins. Symbols represent mean values. Open symbols with arrows indicate minimum lowering rates from erosion pins and emplacement holes that have been entirely removed by erosion. Solid triangles on cross section indicate pins that had no lowering around them. Measurements from different years are shown with different symbols for W.F. Satsop and Black Creek. Base flow measured at time of pin emplacement (less than line thickness at Walker 1), high flow estimated during reoccupation by using stage indicators. Note the absence of pins in the Satsop thalweg, which was too deep to access with a drill. Bedrock lowering at Satsop site occurs by detachment of centimeter-sized weathered fragments during high flow and by abrasion and plucking below base flow. Lowering at Black occurs by detachment of folia like those shown in Figure 3. In these channels, lowering rates decrease and rapidly approach those below base flow. Note that dam-break flood stage lines for Walker Creek occurred before installation, whereas that for Black Creek occurred after pin installation. Large cavity in Black Creek cross section is from an eroded concretion. Aspect ratio is the same for all cross sections.

has been incised meters since levee construction several decades ago (local residents, personal communs.). Engineering structures footed on 1–3-m-high strath terraces at Tali, Tsao-Hu, and Chang-Ping are also consistent with rapid bedrock incision greater than centimeters per year since levee installation along these channels. Modern ceramic fragments in a fill overlying a 1.3-m-high strath in the Chang-Ping River in Taiwan also indicate sustained bedrock-lowering rates of >26 mm/yr, under the assumption of post-1949 emplacement.

Rock Strength

Table 1 shows tensile strengths and slake durabilities for selected sites. Tensile strengths for poorly cemented rocks (i.e., Satsop, Black Creek, Taiwan rivers) were <0.3 MPa. Values for rocks with more cemented or indurated matrixes ranged from 2 to 5 MPa, consistent with measurements of tensile strength for similar lithologies elsewhere (e.g., Goodman, 1980). In Table 1, we characterize the rate of breakdown by showing the number of cycles required for loss of 75% of sample weight. Weak samples required only 1–2 cycles of wetting and drying to lose 75% of their initial weight by slaking (e.g., Satsop, Black Creek, Taiwan samples). For instance, upon immersion after the first drying, samples from Satsop River and Taiwan lost >50% of their mass in the first 5 min. These samples swelled rapidly as water infiltrated matrix, resulting in degassing and millimeter-scale compressional features along their surface. As they expanded, samples comminuted into millimeter-sized aggregations of

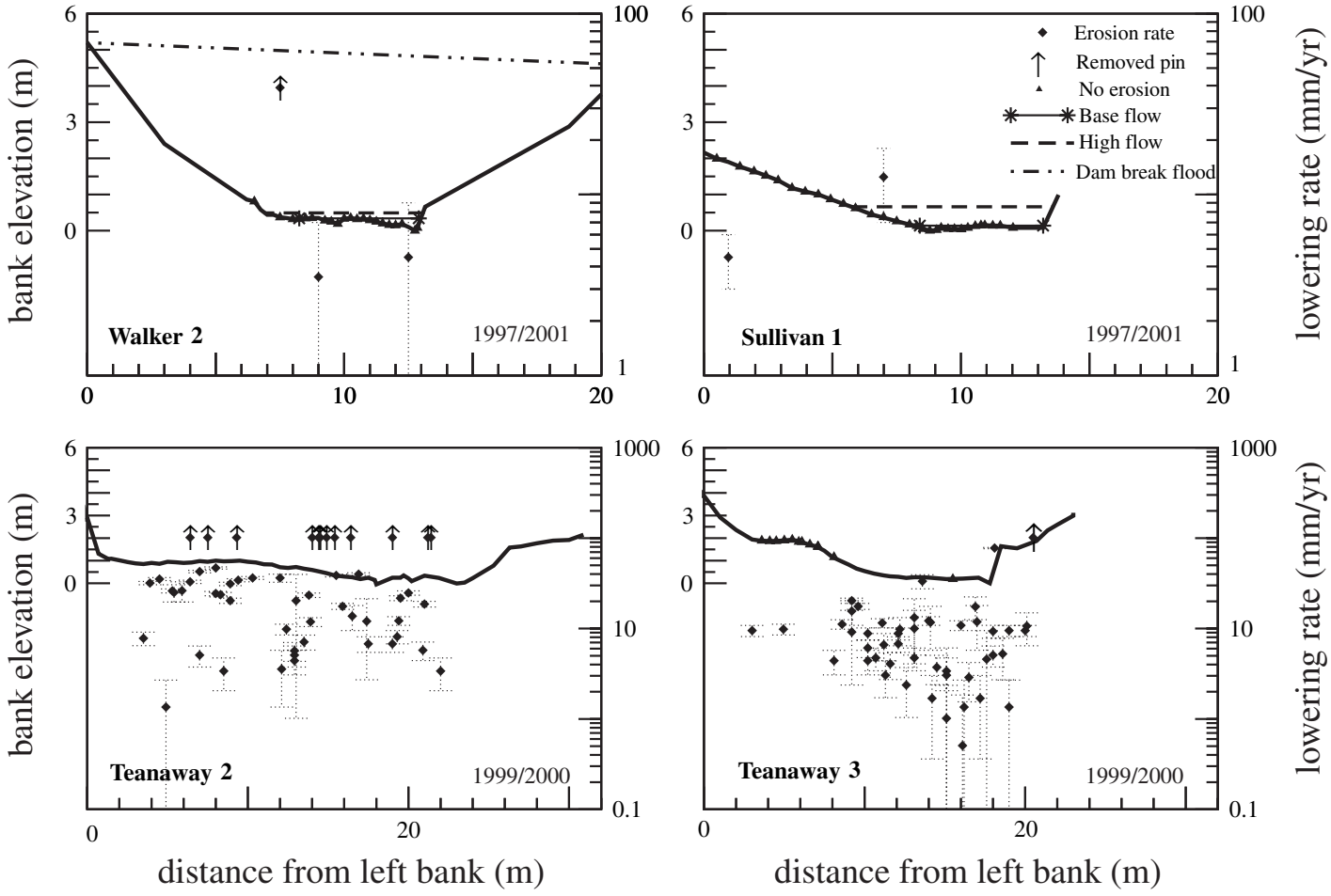

Figure 11. Yearly lowering rates from erosion pins (right y-axis) and cross sections (left y-axis) for Walker Creek 2, Oregon Cascades, Sullivan Creek, Oregon Coast Range, and Teanaway, Washington Cascades. See Figure 10 caption for details. Bedrock lowering in Walker and Sullivan is by removal of local folia and tented folia (e.g., Fig. 3) during high flow, and lowering magnitudes are consistent with folia-depth distributions shown in Figure 13. Lowering at Teanaway is by entrainment of pervasively weathered material (e.g., Fig. 2).

grains that detached from the core and fell at its side. By contrast, samples with tensile strengths of >1 MPa showed little degassing and had only minor degradation after 30 cycles of wetting and drying. We estimated the number of cycles for these stronger rocks (e.g., Walker and Sullivan samples) by regressing mass loss against cycle number. These results are broadly consistent with order-of-magnitude differences in lowering rate recorded in the field.

Figure 14 illustrates the dependence of field-measured bedrock lowering rates on bedrock tensile strength. Although lowering rates for Tachia, Tali, and W.F. Satsop are minimum estimates, the power-law regression with an exponent of approximately –2 is consistent with the inverse-square dependency of erosion rate on tensile strength obtained experimentally by Sklar and Dietrich (2001). Rocks with tensile strengths less than the highest range we tested (3–5 MPa) are lowering at rates that exceed the estimates for regional long-term lowering rates in Table 2.

Area vs. Slope Analysis

Valleys traversed by debris flows (dashed lines in Figs. 15–16) have area vs. slope plots that are curved, largely above slopes of 0.10. For instance, curved data for the unnamed tributary of Sullivan Creek (Fig. 16) correspond to the runout path of the debris flow shown in Figure 9. Curved area vs. slope plots for Sharps and Walker Creeks also occur within reaches with mapped debris-flow deposits. Reaches on both the Sullivan tributary and Walker Creek are now being buried by colluvium and vegetation (e.g., Fig. 9), although they were scoured to bedrock during the 1996–1997 debris flows and dam-break flood on Walker.

Plots of drainage area against slope are approximately log–log-linear in the weak lithologies around most fluvial sites where we have monitored rapid lowering rates and in tributaries with similar lithologies (Figs. 15–16). With the exception of the Tali River, power-law regressions of fluvial erosion-pin sites have concavities between –0.75 and –1.0 and intercepts from 0.08 to 0.70. For instance, reaches cut in sandstone and siltstones of the Satsop (Fig. 15) that weather pervasively (Fig. 2) plot as lines with similar slopes (–0.84 ± 0.07 and –0.78 ± 0.15) and intercepts (0.16 ± 0.07 and 0.10 ± 0.09). Most of these concavity estimates are higher than the values of –0.3 to –0.6 predicted by some stream-power models (Whipple and Tucker, 1999), although they are within the range from –0.2 to –1.3 reported by Stock and Dietrich (2003). Power-law intercepts for these rivers also appear inconsistent

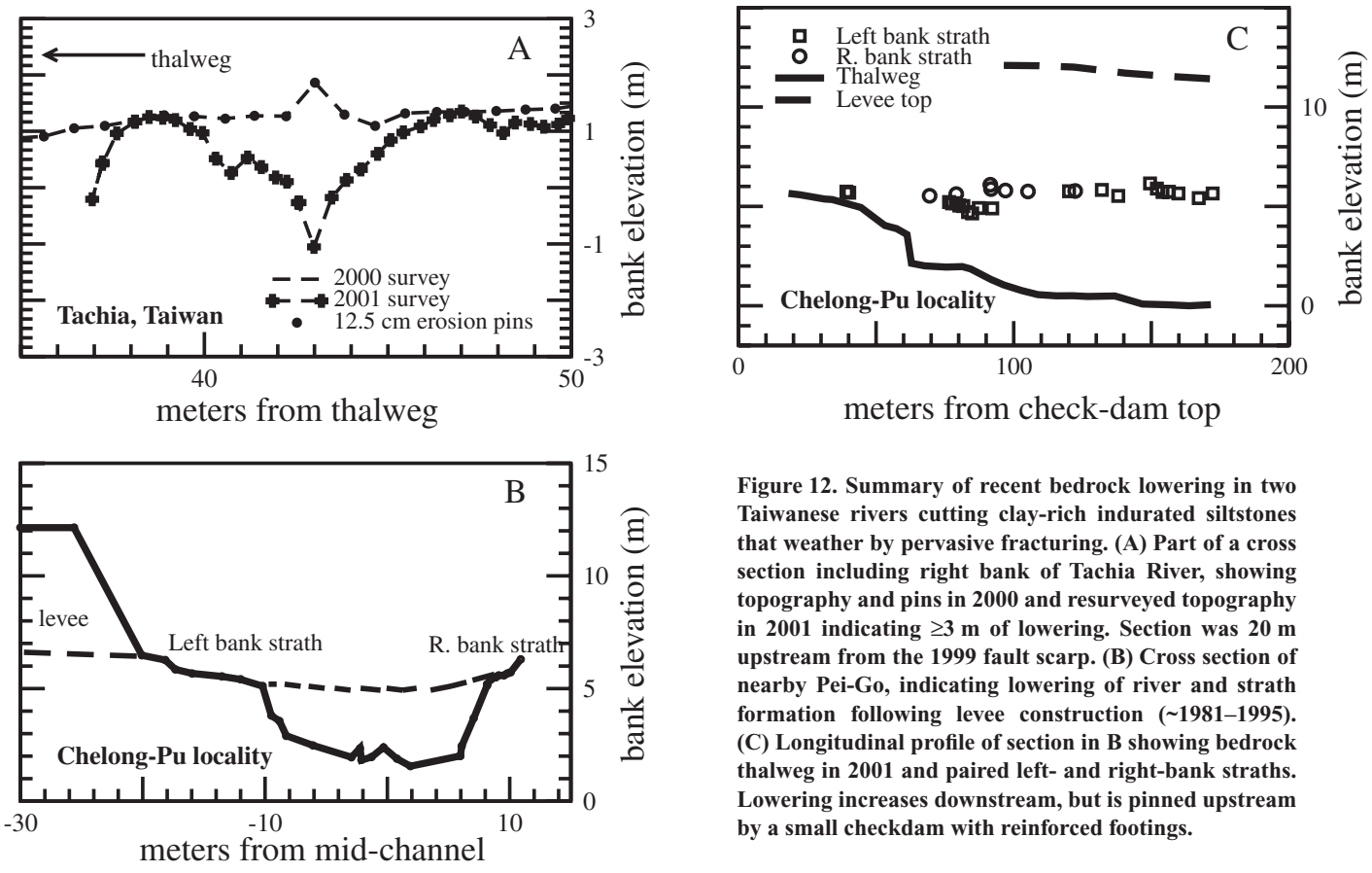

Figure 12. Summary of recent bedrock lowering in two Taiwanese rivers cutting clay-rich indurated siltstones that weather by pervasive fracturing. (A) Part of a cross section including right bank of Tachia River, showing topography and pins in 2000 and resurveyed topography in 2001 indicating ≥3 m of lowering. Section was 20 m upstream from the 1999 fault scarp. (B) Cross section of nearby Pei-Go, indicating lowering of river and strath formation following levee construction (~1981–1995). (C) Longitudinal profile of section in B showing bedrock thalweg in 2001 and paired left- and right-bank straths. Lowering increases downstream, but is pinned upstream by a small checkdam with reinforced footings.

with Equation 1 because they have no apparent relationship to estimates of long-term erosion rate or rock erodibility characterized by tensile strength. For instance, the high intercept of Sharps Creek (0.32) compared to S.F. Eel (0.08), does not correspond to a higher long-term erosion rate for these rocks of similar tensile strength (Table 1). However, substantial uncertainties in rock-uplift rates and other measures of rock resistance to lowering (e.g., fracture density) do not allow us to reject this intercept as a proxy for uplift rate (e.g., Snyder et al., 2000).

There is evidence for transient conditions at some locations. Abrupt local increases in slope within the same mapped lithology occur in Black Creek, Sullivan Creek, and S.F. Eel (Figs. 15–16). In the Eel, these points (open squares in Fig. 16) correspond to the first widespread occurrence of bedrock along the channel. Knickpoints are also present at lithologic boundaries such as the basalt/sandstone contact on the W.F. Satsop (Fig. 15) and mapped outcrops of conglomerates of the Tokoushan Formation upstream of the Chinshui Shale in the Taiwan rivers.

DISCUSSION

Burial of erosion pins in the Sullivan Creek and Marlow Creek debris-flow valleys indicates that fluvial processes are not currently cutting rock or transporting all of the hillslope deposits away. Although it could be argued that future floods might yet lower bedrock, the deep colluvium of adjacent valley floors suggests that burial conditions persist until debris flows or landslides expose and erode the bedrock. For instance, prior to the 1996 debris flow, the bedrock floor of the Sullivan Creek tributary was locally buried by a minimum of 1–3 m of colluvium (unpublished field work by Montgomery). We think that burial in these steep valleys following debris flows is common because during field work in soil-mantled steeplands throughout the Western United States we have generally not seen extensive exposures of bedrock in valley floors above step-pool channels, other than along recent debris-flow tracks. We interpret the rapid burial of erosion pins in the Oregon sites and the dearth of extensive bedrock exposures in steepland valley floors as evidence that debris flows are the primary process lowering the rock in valleys with slopes of >0.10 and curved area vs. slope plots. The curved area vs. slope plots of these valleys are therefore likely to be a signature of debris-flow and weathering processes, with little fluvial contribution.

There is evidence that fluvial erosion occurs in the terminal runout areas of some debris flows, as slopes decline to ~0.10–0.03. For instance, bedrock lowering at Walker and Sullivan Creeks by fluvial entrainment of weathered rock occurred at sites that debris flows had previously crossed. Lowering at both sites was spatially discontinuous as indicated by the abundant folia that had not been mobilized by flow over the monitoring period. These sections are now being covered by sediment (albeit slowly) with a consequent reduction in bedrock exposure. It remains to be seen whether subsequent flows will lower bedrock extensively, or whether cover will be established so quickly that bedrock is weathered but largely uneroded. It is possible that debris flows are the agent of bedrock exposure here, but rivers are the agents of removal following exposure. In this case, the lowermost section of area vs. slope curvature records a combination of fluvial and debris-flow

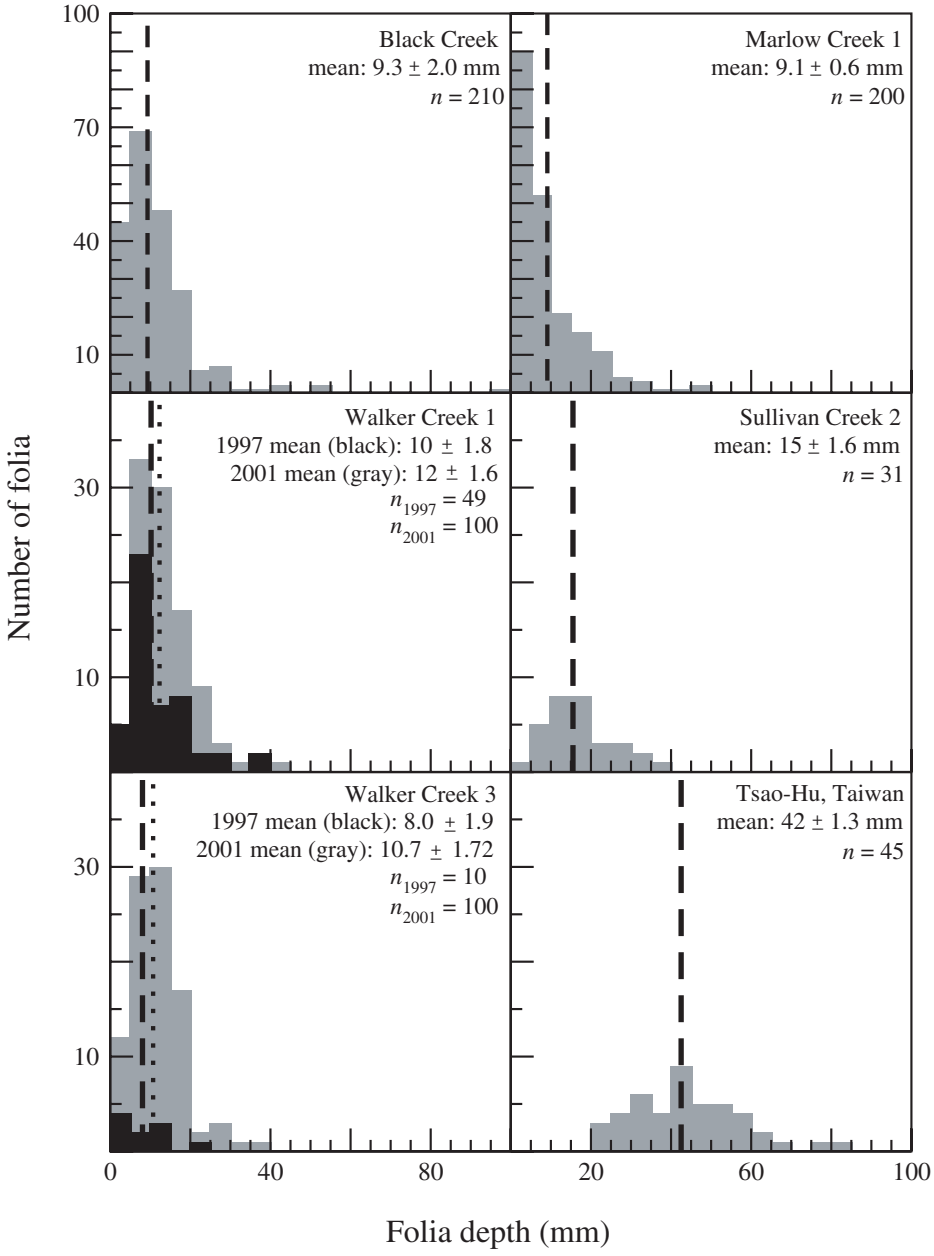

Figure 13. Thickness distributions for weathering folia measured by random walk near erosion-pin cross sections during reoccupation. Black columns are exhaustive samples of folia thicknesses at the time of pin emplacement when the folia are usually less abundant than at reoccupation. Distributions are log normal: few folia are thinner than several millimeters, but there is a long tail of folia thicknesses at hundreds of millimeters. Dashed and dotted (alternate year) lines show log-normal mean values.

processes: debris flows expose bedrock to weathering, and rivers entraining the weathered products. Alternately, debris flows may dominate both exposure and lowering during the subsequent debris flow. Future monitoring at these sites will be necessary to resolve whether cover is largely reestablished, shutting off fluvial entrainment of weathered rock.

In lithologies with tensile strengths below 3–5 MPa, short-term bedrock-incision rates far exceed long-term lowering rates inferred from geologic evidence (Figs. 8 and 14; Table 2). Previous authors have also measured transient river-incision rates in sedimentary rocks of millimeters to centimeters per year that far exceed apparent long-term erosion or rock-uplift rates (Shakoor and Rodgers, 1992; Stock et al., 1996; Righter, 1997; Tinkler and Parrish, 1998; Whipple et al., 2000; Hsieh and Kneupfer, 2001). For instance, Tinkler and Parrish (1998) described the case of an urbanized channel whose recently exposed sedimentary rock appears to weather seasonally via wetting and drying, lowering at centimeters per year. Such rates appear inconsistent with the use of a stream power law to describe the long-term bedrock incision by these rivers because their long profiles cannot steepen if erosion rates can routinely exceed rock-uplift rates whenever rock is exposed. Despite this inconsistency, their long profiles have power-law plots of slope against drainage area (Figs. 15–16), requiring an alternative explanation that we explore in the next section.

A strong dependence of weathering rate on rock tensile strength may partly explain the observed inverse relationship between erosion rate and tensile strength in Figure 14. Given that the correlation reported by Sklar and Dietrich (2001) was for a constant sediment supply rate and grain size, conditions that seem unlikely at our field sites, the similarity between field and laboratory estimates of the regression exponent (–2) may thus be fortuitous. Despite this uncertainty, our results are consistent with the finding by Sklar and Dietrich (1998, 2001) that bed cover strongly modulates fluvial bedrock incision. Gravel-fill terraces at most fluvial sites record the presence of gravel bars and wood jams insulating the bedrock from weathering and abrasion prior to historic disturbance. In most cases, the removal of sediment cover appears to have coincided with the initiation of geologically unsustainable lowering rates. The connection to anthropogenic disturbance is weakest at Sullivan and S.F. Eel, where correspondence of knickpoints with bedrock exposure may indicate prehistoric exposure due to migrating knickpoints.

Rapid lowering above base flow may also limit the channel dimension in these lithologies to bank widths at which base flow for a given discharge is sufficiently deep to insulate bedrock from weathering processes.

Implications for Concavity of Long Profiles

A simple hypothesis to explain the discrepancy between short- and long-term bedrock-lowering rates illustrated in Figure 8 is that in channels where bedrock is so weak that it lowers at rates far in excess of the boundary lowering rate when exposed, slope approaches a value that is low enough so that the rock bed of the river is rarely exposed to erosion for a given hydraulic geometry, peak discharge, grain size, bedform resistance, and sediment supply. This

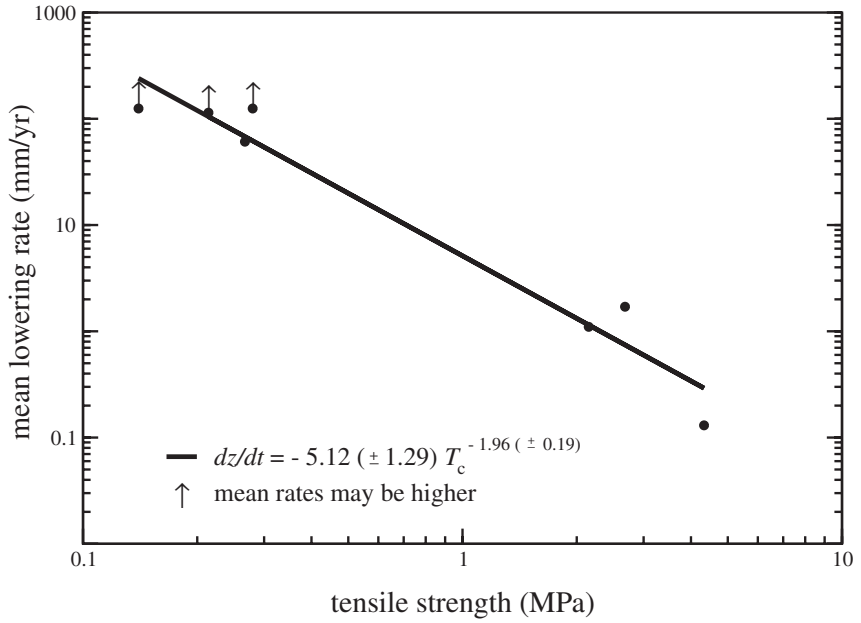

Figure 14. Plot of tensile strength against average lowering rate for sites in Table 2. Arrows indicate minimum lowering rates at sites where many erosion pins were entirely removed. Note that sites whose rocks have tensile strengths of <3–5 MPa are eroding at rates that appear to exceed long-term rates from geologic indicators.

could be called "exposure-limited erosion." Howard (1980) proposed a simple expression to predict the long profile of threshold gravel-bedded rivers, independent of sediment supply and bedform roughness. Below, we use a more explicit version of his analysis to explore what such a relationship would predict for rivers where we have monitored rapid lowering and have reconnaissance width data (Table 3). The intent is to demonstrate how we might expect hydraulic geometry and grain size to influence area vs. slope plots like that of Figure 1, not necessarily to predict accurate concavity values because we lack methods of adequately characterizing or estimating bed load sediment supply and total flow resistance along the network. We approximate both channel width and grain size as power laws solely to characterize observed tendencies for downstream fining and widening, both of which may be locally violated by changes in lithology or sediment supply.

Following Howard (1980), we assume threshold conditions for gravel transport at channel-forming stages so that Shields' criterion predicts that at the threshold of motion for a uniform grain size D,

$$\tau_c = \tau^*_c(\rho_r - \rho_w)gD\,, \qquad (2)$$

where ρ_r and ρ_w are sediment particle and water density, g is gravitational constant, τ_c is critical fluid shear stress, and τ^*_c is a dimensionless number characterizing resistance to motion. Approximations of τ_c using the product of hydraulic radius R and slope S ($\rho_w gRS$) are known to be locally inaccurate, but may capture network-scale variations in transport capacity. This approximation allows equation 2 to be recast as

$$S = \tau^*_c\left[\frac{\rho_r - \rho_w}{\rho_w}\right]\frac{D}{R}\,. \qquad (3)$$

If the variation in hydraulic radius and grain size with drainage area are known, the threshold channel condition can be inverted for a long profile. U.S. Geological Survey gaging records in the field areas (Table 3) indicate that for mean annual peak discharges (floods of 2.33 yr recurrence intervals)

$$Q_{ma} = c_1 A^{\theta_1}, \quad 0.8 < \theta_1 < 1.2\,. \qquad (4)$$

We characterize mean annual floods rather than 1.5 yr recurrence-interval peak discharges because the smaller discharges often just fill the channel banks leading to initiation of gravel transport (e.g., Parker, 1979; Buffington and Montgomery, 1997). Mean annual floods are more likely to entrain coarser fractions (e.g., Andrews, 1983) that seem critical for bed exposure. Lower-frequency floods may be more relevant, but we found that available gaging station records are rarely long enough to characterize them well, leading to non–power-law regressions. Nonetheless, many channels are covered by clasts that appear to be less frequently moved, particularly in step-pool reaches. Field measurements of channel bank width (e.g., Montgomery and Gran, 2001; Tables 1 and 3) in relatively uniform lithology indicate that

$$w_b = c_2 A^{\theta_2}, \quad 0.3 < \theta_2 < 0.6\,. \qquad (5)$$

We parameterize grain size as

$$D_n = c_3 A^{\theta_3}, \quad -0.6 < \theta_3 < 0.0\,, \qquad (6)$$

where D_n is the nth percentile of a grain-size distribution and illustrative θ_3 values come from Appalachian rivers studied by Brush (1961). For the purposes of predicting an area vs. slope relationship for such a threshold channel, we use the following relationships: (a) $R = h$, where h is depth; (b) $U_{av} = (R^{2/3}S^{1/2})/n$, where n is Manning's resistance coefficient; (c) $h = Q_{ma}/U_{av}w_b$, where Q_{ma} is mean annual discharge (assumed to be the 2.33 yr recurrence-interval discharge) and w_b is bank width; and (d) τ^*_c is a constant between 0.03 and 0.06 (e.g., Buffington and Montgomery, 1997).

Excluding channels influenced by debris flows, the width to depth ratio is mostly >17 for our field sites, so R is closely approximated by flow depth. We approximate τ^*_c as 0.047, although some have suggested that the Shields number might vary with slope (Shvidchenko and Pender, 2000). Substituting the expression for velocity into the expression for h as a function of discharge yields the depth of flow at entrainment of a uniform grain size D:

$$R = h = (Q_{ma}^{3/5} n^{3/5})/S^{3/10} w_b^{3/5}\,. \qquad (7)$$

Substituting equation 7 into equation 3 and rearranging for S yields

$$S = \left[\frac{\tau^*_c}{n^{3/5}}\left[\frac{\rho_r - \rho_w}{\rho_w}\right]\right]^{10/7}\left[\left(\frac{w_b}{Q_{ma}}\right)^{3/5} D\right]^{10/7}\,. \qquad (8)$$

This expression predicts that slope of a channel in which the selected grain size approaches initial motion will be a function of some relatively immobile grain size D_n common enough to cover substantial parts of the bed, as well as channel width and discharge. However, we know of no field studies that address the relevant grain-size issue, although it is apparent that supply may vary strongly within basins (e.g., Pizzuto, 1995). By approximating variables in equation 8 as functions of drainage area, we can predict the form of an equilibrium area vs. slope plot for such a river by substituting equations 4, 5, and 6 into equation 8:

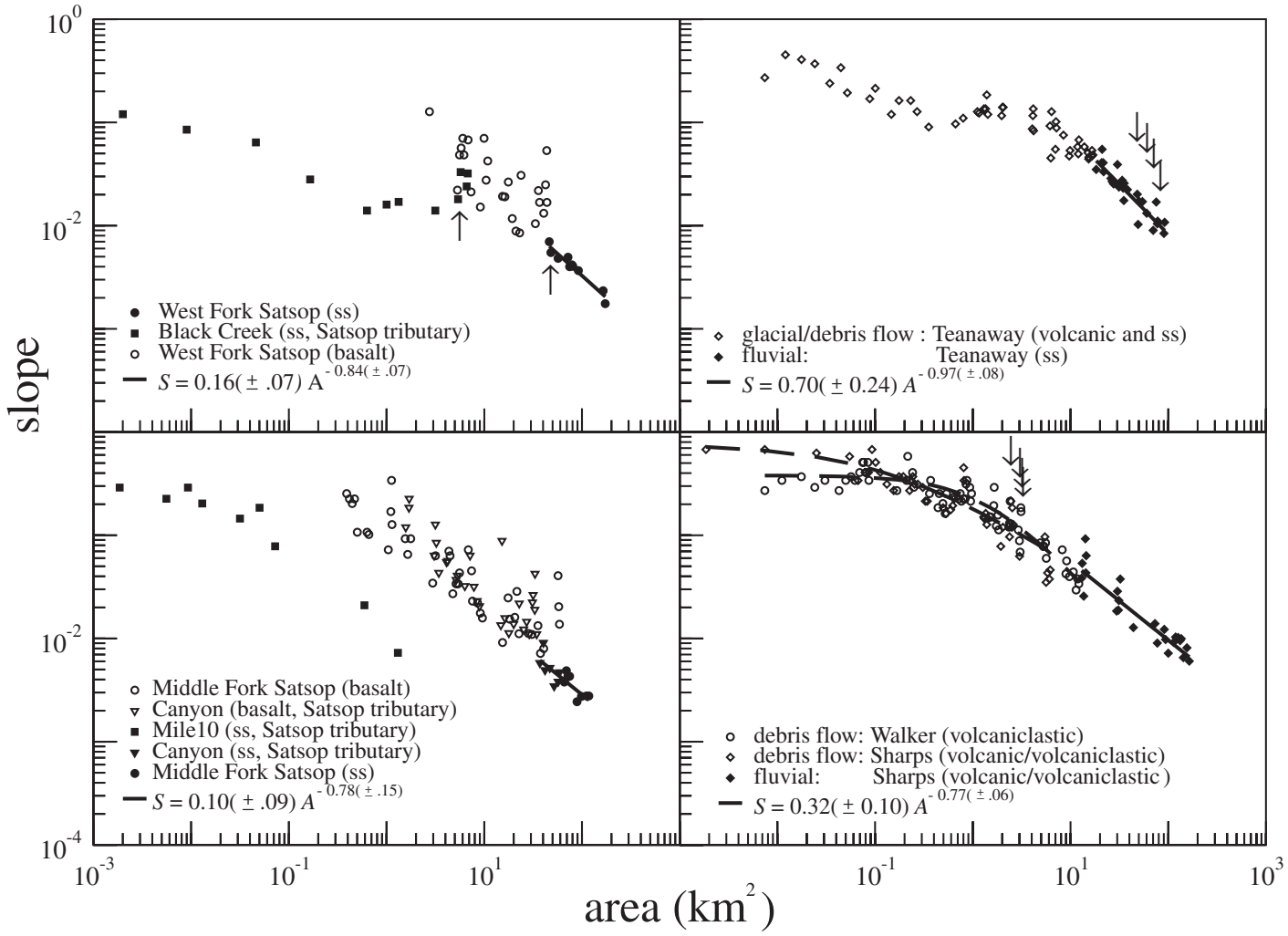

Figure 15. Plot of slope against area for sites in the first three regions of Table 2. Infilled squares, diamonds, and triangles indicate fluvial reaches in lithologies where we have measured lowering rates with erosion pins. Note that we fit power laws only to reaches within lithologies with measured lowering rates. Stars, X's, and pluses indicate lithologies where we did not have erosion pins (e.g., basalt). Open diamonds and triangles indicate the mapped extent of debris-flow deposits and were fit with an empirical slope-area relationship (dashed line) that curves (see Fig. 1 legend). Arrows indicate the location of erosion-pin cross sections. Lower left panel presents data from basins tributary to the W.F. Satsop, that lack erosion-pin sites, but that occur in similar lithologies.

$$S = k_1 A^{\theta}, \qquad (9a)$$

where

$$\theta = \frac{6}{7}(\theta_2 - \theta_1) + \frac{10}{7}\theta_3, \qquad (9b)$$

and

$$k_1 = \left[\frac{\tau_c^*}{n^{3/5}}\left[\frac{\rho_r - \rho_w}{\rho_w}\right]\right]^{10/7}\left(\frac{c_2}{c_1}\right)^{6/7} c_3^{10/7}. \qquad (9c)$$

Equation 9b predicts that the magnitude of concavity increases as discharge and grain size change more rapidly with drainage area (larger absolute values of θ_1 and θ_3, respectively) and decreases as width increases more rapidly with drainage area (larger positive θ_2 values). The intercept k_1 increases as width and grain size at a reference drainage area increase, and decreases as discharge increases at the reference area. Equation 9b predicts concavities from –0.2 to –1.2 by using commonly observed ranges of hydraulic and grain-size exponents in equations 4, 5, and 6. These values span the same range observed across many different rock types and climates (e.g., Stock and Dietrich, 2003). Table 3 illustrates almost as great a range of θ resulting from combining site-specific values of θ_1 and θ_2 with the range of reported θ_3 values in Equation 6. Alternately, θ values from area vs. slope data can be used to predict a reasonable range of θ_3 values between ~–0.1 and –0.3. These crude calculations suggest that long-profile concavities and intercepts now widely interpreted in terms of Equation 1 (e.g., Snyder et al., 2000; Kirby and Whipple, 2001) could be explained for some channels in alternate ways that are more consistent with field observations of very rapid bedrock lowering. The preceding analysis is consistent with the hypothesis that in channels cutting through weak rock, slope approaches a value that is low enough that the rock bed of the river is rarely exposed to erosion for a given set of hydraulic conditions (e.g., peak discharge, grain size, bedform resistance, and sediment supply). For instance, the higher intercept for Sharps Creek in Figure 1 may

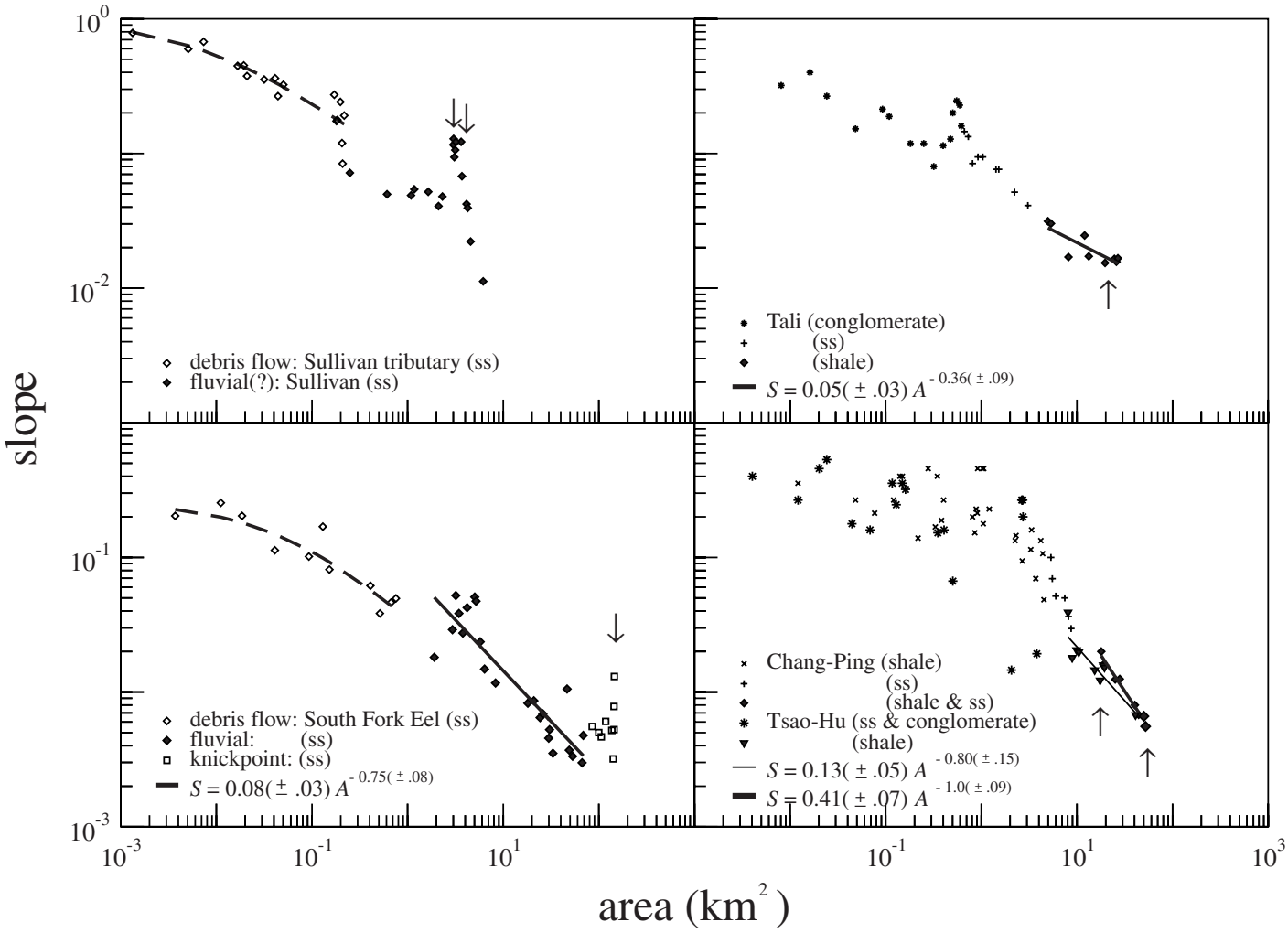

Figure 16. Plot of slope against area for the last three regions of Table 2. See Figure 15 caption for details. Erosion-pin cross sections are too dense (every ~20 m) to show on the Sullivan Creek tributary; see Figure 4 for approximate locations. Sullivan Creek tributary data (from laser altimetry) include runout path shown in Figure 9. Note that we have excluded the downstream-most reaches of S.F. Eel (open squares), from regression because they occur in reaches influenced by knickpoints with common bedrock exposure (unlike reaches in the log–log-linear section).

TABLE 3. HYDRAULIC DATA FOR SELECTED RIVERS

Stream	$Q_{2.33} = c_1 A^{\theta_1}$	USGS gage numbers used	$w_{bf} = c_2 A^{\theta_2}$	θ range if $0 < \theta_3 < -0.6$	θ from Figures 15–16	Predicted θ_3
West Fork, Satsop	$0.89A^{1.0}$	12059500, –68500, –61500, –60500, –39500, –39000, –37400, –36000, –35400, –32500, –35000	$7A^{0.47}$	–0.45 to –1.30	–0.84	–0.27
Teanaway	$0.05A^{1.2}$	12488500, –76000, –58000, –51500, –51000	$1.12A^{0.60}$	–0.51 to –1.36	–0.97	–0.32
Sharp	$0.69A^{0.99}$	14152500, –150300, –151000, –156500, –316700, –318000	$5.4A^{0.29}$	–0.60 to –1.45	–0.77	–0.12
South Fork, Eel	$2.0A^{0.86}$	11478500, –73900, –75560, –75800, –76500, –80500, –72200, –72150, –68500, –68000, –75500, –75000	$2.9A^{0.48}$	–0.33 to –1.18	–0.75	–0.3

reflect a coarser imposed grain size than that of the Teanaway, rather than a higher rock-uplift rate or harder rock. Patterns in slope across rising anticlines may reflect transport conditions in confined, narrower channels, rather than a signal for rock-uplift rate.

This alternate view of some bedrock rivers is not solely an academic debate because anthropogenic changes in sediment supply that would reduce bed cover are widespread, particularly where dams impound coarse sediment. Stock has observed a total of ~5 m of historic incision into siltstones of the Moravka River in the Czech Republic, downstream from a twentieth-century dam. Continuation of this incision puts one of the more biologically diverse floodplains of Europe at risk of being converted into a bedrock gorge. It is likely that many other flood-plain

systems with shallow cover over weak bedrock are also at risk. Reducing these incision rates while maintaining a natural channel ecosystem will require the ability to calculate the sediment load and grain-size distribution necessary to maintain cover, an ability we lack at present.

CONCLUSION

Field observations offer strong support to (1) the interpretation that debris flows dominate steep channel incision, at least above slopes of ~0.10, and (2) the theoretical results from Sklar and Dietrich (1998, 2001) that sediment cover and grain size dominate river-channel gradients. Both findings demonstrate that the stream power law is too simple and provides insufficient insight about the mechanisms that control valley incision.

Valleys recently scoured by debris flows in the Oregon Coast Range have curved area vs. slope plots that are likely to be signatures for debris-flow incision alone (Stock and Dietrich, 2003), because no fluvial lowering occurred in these valleys before hillslope sediment began reburying hundreds of erosion pins. On the other hand, minor fluvial entrainment of weathered rock along the downstream-most debris-flow runout at Walker Creek indicates that fluvial incision could contribute in a transition region having a slope range of 0.04–0.10 at this site. It remains to be seen whether reburial will prevent substantial fluvial lowering of weathered rock.

Very high incision rates of millimeters to decimeters per year in river reaches having recently exposed bedrock support the argument by Sklar and Dietrich (1998, 2001) that sediment coverage dramatically inhibits erosion rates. Given that these rates appear to exceed long-term estimates of lowering rates, this result indicates that at the very least, rates of river incision in weak lithologies (<3–5 MPa) may be limited by the frequency of exposure rather than by stream power, as is assumed in most landscape-evolution models. Lowering data also provide some field verification of the dependency of bedrock lowering on the square of rock tensile strength, proposed by Sklar and Dietrich (2001) on the basis of flume experiments.

We suggest that in the case of mechanically weak rocks in which the coarse-sediment supply also undergoes considerable breakdown during transport, the channel slope is neither set by bedrock strength nor by sediment supply, but instead primarily by the threshold motion of some characteristic grain size. The large concavities (–0.7 to –1.0) observed in our field sites may be due to the predominance of this sediment threshold of motion and to downstream fining. Where this condition occurs, there may be little variation in long profiles across rock-uplift rates and no direct expression of the bedrock-incision law on river longitudinal profiles. Instead, power-law plots of slope against area may reflect the long-term control by discharge, width, slope, and sediment supply of an alluvial cover sufficiently thin to insulate the bed from drying, abrasion, or weathering processes. Because coverage is largely dictated by the quantity and size distribution of sediment, as well as by hydraulics, these variables may be dominant controls on even apparently bedrock-dominated long profiles.

ACKNOWLEDGMENTS

We gratefully acknowledge the inspiration and field help of N.P. Peterson. Kevin Schmidt and Cliff Riebe also helped install erosion pins. We thank Meng-Long Hsieh and colleagues at National University of Taiwan for their invaluable guidance and assistance in field work in Taiwan. We thank Chad Pedrioli for measuring much of the area vs. slope data. We thank Tracy Allen for supplying stage data for the Branscomb gage on the Eel River. We thank David Finlayson, Karen Gran, the Kapor family, Taylor Perron, Joel Rowland, Xena T. Dog, Elowyn Yager, and Paul Zelfus for field assistance. We thank Steven Lancaster and Alan Howard for generous reviews. Stock was inspired to install erosion pins after watching Robert Anderson's efforts on marine terraces at University of California, Santa Cruz. Stock thanks NASA (National Aeronautical and Space Administration) SRTM NAG5-9629 for support; support for Sklar came from National Science Foundation STC: National Center for Earth-Surface Dynamics.

REFERENCES CITED

Anderson, R.S., 1994, Evolution of the Santa Cruz Mountains, California, through tectonic growth and geomorphic decay: Journal of Geophysical Research, v. 99, p. 20,161–20,179, doi: 10.1029/94JB00713.

Andrews, E.D., 1983, Entrainment of gravel from naturally sorted riverbed material: Geological Society of America Bulletin, v. 94, p. 1225–1231.

ASTM (American Society for Testing and Materials), 1997, Standard test method for evaluation of durability of rock for erosion under wetting and drying conditions: Annual Book of ASTM Standards, Volume 04.08, Designation D, v. 5313-92, p. 1148.

Baldwin, J.A., Whipple, K.X., and Tucker, G.E., 2003, Implications of the shear stress river incision model for the timescale of postorogenic decay of topography: Journal of Geophysical Research, v. 108, no. B3, 2158, doi: 10.1029/2001JB000550.

Brandon, M.T., Roden-Tice, M.K., and Garver, J.I., 1998, Late Cenozoic exhumation of the Cascadia accretionary wedge in the Olympic Mountains, NW Washington State: Geological Society of America Bulletin, v. 110, p. 985–1009.

Brush, L.M., Jr., 1961, Drainage basins, channels, and flow characteristics of selected streams in central Pennsylvania: U.S. Geological Survey Professional Paper 282-F, p. 145–181.

Buffington, J.M., and Montgomery, D.R., 1997, A systematic analysis of eight decades of incipient motion studies, with special reference to gravel-bedded rivers: Water Resources Research, v. 33, p. 1993–2029, doi: 10.1029/97WR03190.

Chang, J.-C., and Slaymaker, O., 2002, Frequency and spatial distribution of landslides in a mountainous drainage basin: Western Foothills, Taiwan: CATENA, v. 46, p. 285–307, doi: 10.1016/S0341-8162(01)00157-6.

Chen, Y.-G., and Liu, T.-K., 1991, Radiocarbon dates of river terraces along the lower Tahanchi, northern Taiwan: Their tectonic and geomorphic implications: Journal of the Geological Society of China, v. 34, p. 337–347.

Collins, B.D., Montgomery, D.R., and Haas, A.D., 2002, Historical changes in the distribution and functions of large wood in Puget Lowland rivers: Canadian Journal of Fisheries and Aquatic Sciences, v. 59, p. 66–76, doi: 10.1139/F01-199.

Davy, P., and Crave, A., 2000, Upscaling local-scale transport processes in large-scale relief dynamics: Physics and Chemistry of the Earth, Ser. A, v. 25, p. 533–541, doi: 10.1016/S1464-1895(00)00082-X.

Day, R.W., 1994, Weathering of expansive sedimentary rock due to cycles of wetting and drying: Bulletin of the Association of Engineering Geologists, v. 31, p. 387–390.

Dendy, F.E., and Champion, W.A., 1978, Sediment deposition in U.S. reservoirs, Summary of data reported through 1975: U.S. Department of Agriculture Miscellaneous Publication 1362, 82 p.

Dick, J.C., and Shakoor, A., 1992, Lithologic controls of mudrock durability: Quarterly Journal of Engineering Geology, v. 25, p. 31–46.

Fujiwara, K., 1970, A study on the landslides by aerial photographs: Research Bulletins of the College Experiment Forests: Hokkaido, Japan, Hokkaido University, v. 27, p. 297–345.

Gasparini, N.M., Tucker, G.E., and Bras, R., 1999, Downstream fining through selective particle sorting in an equilibrium drainage network: Geology, v. 27, p. 1079–1082, doi: 10.1130/0091-7613(1999)0272.3.CO:2.

Goodman, R.E., 1980, Introduction to rock mechanics: New York, Wiley, 478 p.

Haskins, D.R., and Bell, F.G., 1995, Drakensberg basalts: Their alteration, breakdown and durability: Quarterly Journal of Engineering Geology, v. 28, p. 287–302.

Heimsath, A.M., Dietrich, W.E., Nishiizumi, K., and Finkel, R.C., 2001, Stochastic processes of soil production and transport: Erosion rates, topographic variation, and cosmogenic nuclides in the Oregon Coast Range: Earth Surface Processes and Landforms, v. 26, p. 531–552, doi: 10.1002/ESP.209.

Ho, H.-C., and Chen, M.-M., 2000, Geologic map of Taichung (sheet 24): Taiwan Central Geological Survey, scale 1:50,000.

Hofmeister, R.J., 2000, Slope failures in Oregon: GIS inventory for three 1996/97 storm events: Oregon, Department of Geology and Mineral Industries Special Paper 34, 20 p.

Howard, A.D., 1980, Thresholds in river regimes, *in* Coates, D.R., and Vitek, J.D., eds., Thresholds in geomorphology: London, Allen and Unwin, p. 227–258.

Howard, A., and Kerby, G., 1983, Channel changes in badlands: Geological Society of America Bulletin, v. 94, p. 739–752.

Hsieh, M.-L., and Kneupfer, P.L.K., 2001, Middle-late Holocene river terraces in the Erhjen River Basin, southwestern Taiwan—Implications of river response to climate change and active tectonic uplift: Geomorphology, v. 38, p. 337–372, doi: 10.1016/S0169-555X(00)00105-7.

Julien, P.Y., 1998, Erosion and sedimentation: Cambridge, UK, Cambridge University Press, 280 p.

Kao, H., and Chen, W.-P., 2000, The Chi-Chi earthquake sequence: Active, out-of-sequence thrust faulting in Taiwan: Science, v. 288, p. 2346–2349, doi: 10.1126/SCIENCE.288.5475.2346.

Kirby, E., and Whipple, K.X, 2001, Quantifying differential rock-uplift rates via stream profile analysis: Geology, v. 29, p. 415–418, doi: 10.1130/0091-7613(2001)0292.0.CO:2.

Kirby, E., Whipple, K.X, Tang, W., and Chen, Z., 2003, Distribution of active rock uplift along the eastern margin of the Tibetan Plateau: Inferences from bedrock channel longitudinal profiles: Journal of Geophysical Research, v. 108, no. B4, 2217, doi: 10.1029/2001JB000861.

Kusumi, H., Nishida, K., Matsushita, C., and Teraoka, K., 1998, Shear behavior of soft rock exposed to alternate dry and wet under constant stresses, *in* Evangelista, A., and Picarelli, L., eds., Geotechnics of hard soils–soft rocks: Balkema, Rotterdam, p. 253–258.

Lave, J., and Avouac, J.P., 2001, Fluvial incision and tectonic uplift across the Himalayas of central Nepal:

Journal of Geophysical Research, v. 106, no. B11, p. 26,561–26,591, doi: 10.1029/2001JB000359.
Li, Y.-H., 1976, Denudation of Taiwan Island since the Pliocene Epoch: Geology, v. 4, p. 105–107.
Liu, T.-K., Hsieh, S., Chen, Y.-G., and Chen, W.-S., 2001, Thermo-kinematic evolution of the Taiwan oblique-collision mountain belt as revealed by zircon fission track dating: Earth and Planetary Science Letters, v. 186, p. 45–56, doi: 10.1016/S0012-821X(01)00232-1.
McIntosh, B.A., Clark, S.E., and Sedell, J.R., 1995, Summary report for Bureau of Fisheries stream habitat surveys, Yakima River Basin 1934–1942: Report to U.S. Department of Energy, Bonneville Power Administration, Report DOE/BP-02246–5, 311 p.
Merritts, D., and Vincent, K.R., 1989, Geomorphic response of coastal streams to low, intermediate, and high rates of uplift, Mendocino triple junction region, northern California: Geological Society of America Bulletin, v. 101, p. 1373–1388.
Milliman, J.D., and Syvitski, J.P.M., 1992, Geomorphic/tectonic control of sediment discharge to the ocean: The importance of small mountainous rivers: Journal of Geology, v. 100, p. 525–544.
Miscevic, P., 1998, The investigation of weathering process in Eocene flysch, *in* Evangelista, A., and Picarelli, L., eds., Geotechnics of hard soils–soft rocks: Balkema, Rotterdam, p. 267–272.
Montgomery, D.R., and Dietrich, W.E., 1992, Channel initiation and the problem of landscape scale: Science, v. 255, p. 826–830.
Montgomery, D.R., and Foufoula-Georgiou, E., 1993, Channel network source representation using digital elevation models: Water Resources Research, v. 29, p. 3925–3934, doi: 10.1029/93WR02463.
Montgomery, D.R., and Gran, K.B., 2001, Downstream variations in the width of bedrock channels: Water Resources Research, v. 37, p. 1841–1846, doi: 10.1029/2000WR900393.
Montgomery, D.R., Abbe, T.B., Buffington, J.M., Peterson, N.P., Schmidt, K.M., and Stock, J.D., 1996, Distribution of bedrock and alluvial channels in forested mountain drainage basins: Nature, v. 381, p. 587–589, doi: 10.1038/381587A0.
Montgomery, D.R., Massong, T.M., and Hawley, S.C.S., 2003, Debris flows, log jams and the formation of pools and alluvial channel reaches in the Oregon Coast Range: Geological Society of America Bulletin, v. 115, p. 78–88, doi: 10.1130/0016-7606(2003)1152.0.CO:2.
Moon, V.G., and Beattie, A.G., 1995, Textural and microstructural influences on the durability of Waikato Coal Measures mudrocks: Quarterly Journal of Engineering Geology, v. 28, p. 303–312.
Mugridge, S.-J., and Young, H.R., 1983, Disintegration of shale by cyclic wetting and drying and frost action: Canadian Journal of Earth Sciences, v. 20, p. 568–576.
Parker, G., 1979, Hydraulic geometry of active gravel rivers: Journal of the Hydraulics Division, v. 105, p. 1185–1201.
Personious, S.F., 1995, Late Quaternary stream incision and uplift in the forearc of the Cascadia subduction zone, western Oregon: Journal of Geophysical Research, v. 100, p. 20,193–20,210, doi: 10.1029/95JB01684.
Pizzuto, J.E., 1995, Downstream fining in a network of gravel-bedded rivers: Water Resources Research, v. 31, p. 753–759, doi: 10.1029/94WR02532.
Reiners, P.W., Ehlers, T.A., Garver, J.I., Mitchell, S.G., Montgomery, D.R., Vance, J.A., and Nicolescu, S., 2002, Late Miocene exhumation and uplift of the Washington Cascades: Geology, v. 30, p. 767–770, doi: 10.1130/0091-7613(2002)0302.0.CO:2.
Reneau, S.L., and Dietrich, W.E., 1991, Erosion rates in the southern Oregon Coast Range—Evidence for an equilibrium between hillslope erosion and sediment yield: Earth Surface Processes and Landforms, v. 16, p. 307–322.
Righter, K., 1997, High bedrock river incision rates in the Agenguillo River Valley, Jalisco, western Mexico: Earth Surface Processes and Landforms, v. 22, p. 337–343, doi: 10.1002/(SICI)1096-9837(199704)22:43.3.CO:2-T.
Rubin, C.M., Sieh, K., Chen, Y.-G., Lee, J.-C., Chu, H.-T., Yeats, R., Mueller, K., and Chan, Y.-C., 2001, Surface rupture and behavior of thrust faults probed in Taiwan: Eos (Transactions, American Geophysical Union), v. 82, p. 565, 569.
Russell, I.C., 1898, Rivers of North America: New York, G.P. Putnam & Sons, 327 p.
Santi, P.M., and Shakoor, A., 1997, Characterization of weak and weathered rock masses: Association of Engineering Geologists Special Publication 9, 233 p.
Sedell, J.R., and Luchessa, K.J., 1981, Using the historical record as an aid to salmonid habitat enhancement, *in* Armantrout, N.B., ed., Acquisition and utilization of aquatic habitat inventory information: American Fisheries Society, p. 210–223.
Seidl, M.A., and Dietrich, W.E., 1992, The problem of channel erosion into bedrock, *in* Schmidt, K.-H., and DePloey, J., eds., Functional geomorphology: Catena Supplement 23, p. 101–124.
Seidl, M.A., Dietrich, W.E., and Kirchner, J.W., 1994, Longitudinal profile development into bedrock—An analysis of Hawaiian channels: Journal of Geology, v. 102, p. 457–474.
Shakoor, A., and Rodgers, J.P., 1992, Predicting the rate of shale undercutting along highway cuts: Bulletin of Engineering Geology, v. 24, p. 61–75.
Sherrod, D.R., and Smith, J.G., 2000, Geologic map of upper Eocene to Holocene volcanic and related rocks of the Cascade Range, Oregon: U.S. Geological Survey Map I-2569, scale 1:500,000.
Shideler, J.C., 1986, Coal towns in the Cascades: A centennial history of Roslyn and Cle Elum, Washington: Spokane, Washington, Melior Publications, 151 p.
Shvidchenko, A.B., and Pender, G., 2000, Flume study of the effect of relative depth on the incipient motion of coarse uniform sediments: Water Resources Research, v. 36, p. 619–628, doi: 10.1029/1999WR900312.
Sklar, L.S., and Dietrich, W.E., 1998, River longitudinal profiles and bedrock incision models: Stream power and the influence of sediment supply, *in* Tinkler, K.J., and Wohl, E.E., eds., Rivers over rock: Fluvial processes in bedrock channels: American Geophysical Union Geophysical Monograph 107, p. 237–260.
Sklar, L.S., and Dietrich, W.E., 2001, Sediment and rock strength controls on river incision into bedrock: Geology, v. 29, p. 1087–1090, doi: 10.1130/0091-7613(2001)0292.0.CO:2.
Snyder, N.P., Whipple, K.X, Tucker, G.E., and Merritts, D.J., 2000, Landscape response to tectonic forcing: Digital elevation model analysis of stream profiles in the Mendocino triple junction region, northern California: Geological Society of America Bulletin, v. 112, p. 1250–1263, doi: 10.1130/0016-7606(2000)1122.3.CO:2.
Sommerfield, C.K., Drake, D.E., and Wheatcroft, R.A., 2002, Shelf record of climatic changes in flood magnitude and frequency, north-coastal California: Geology, v. 30, p. 395–398, doi: 10.1130/0091-7613(2002)0302.0.CO:2.
Stock, J.D., 2004, Incision of Steepland Valleys by Debris Flows: Berkeley, University of California, 245 p.
Stock, J.D., and Dietrich, W.E., 2003, Valley incision by debris flows: Evidence of a topographic signature: Water Resources Research, v. 39, no. 4, 1089, doi: 10.1029/2001WR001057.
Stock, J.D., and Montgomery, D.R., 1999, Geologic constraints on bedrock river incision using the stream power law: Journal of Geophysical Research, v. 104, p. 4983–4993, doi: 10.1029/98JB02139.
Stock, J.D., Montgomery, D.R., and Peterson, N.P., 1996, Extreme rates of bedrock river incision, Satsop River, Washington: Eos (Transactions, American Geophysical Union), v. 77, p. F252.
Sung, Q., You, S.-Y., and Liao, J.-Y., 1995, Correlation of river terraces by quantitative morphological dating and its neotectonic implications: Journal of the Geological Society of China, v. 38, p. 65–80.
Sung, Q., Lu, M.-T.L., Tsai, H., and Liew, P.-M., 1997, Discussion of the genetics and the correlation of river terraces in Taiwan: Journal of the Geological Society of China, v. 40, p. 31–46.
Tabor, R.W., and Cady, W.M., 1978, Geologic map of the Olympic Peninsula: U.S. Geological Survey Map I-994, scale 1:125,000.
Tabor, R.W., Frizzell, V.A., Jr., Booth, D.B., and Waitt, R.B., 2000, Geologic map of the Snoqualmie Pass 30 × 60 minute Quadrangle, Washington: U.S. Geological Survey Map I-2538, scale 1:100,000.
Taylor, R.K., and Cripps, J.C., 1987, Weathering effects: Slopes in mudrocks and overconsolidated clays, *in* Anderson, M.G., and Richards, K.S., eds., Slope stability: Chichester, UK, John Wiley & Sons, p. 405–445.
Taylor, R.K., and Smith, T.J., 1986, The engineering geology of clay minerals: Swelling, shrinking and mudrock breakdown: Clay Minerals, v. 21, p. 235–260.
Tinkler, K.J., and Parrish, J., 1998, Recent adjustments to the long profile of Cook Creek, an urbanized bedrock channel in Mississauga, Ontario, *in* Tinkler, K.J., and Wohl, E.E., eds., Rivers over rock: Fluvial processes in bedrock channels: American Geophysical Union Geophysical Monograph 107, p. 167–188.
Tucker, G.E., and Slingerland, R., 1996, Predicting sediment flux from fold and thrust belts: Basin Research, v. 8, p. 329–349, doi: 10.1046/J.1365-2117.1996.00238.X.
Tucker, G.E., and Whipple, K.X, 2002, Topographic outcomes predicted by stream erosion models: Sensitivity analysis and intermodel comparison: Journal of Geophysical Research, v. 107, no. B9, 2179, doi: 10.1029/2001JB000162.
Vutukuri, V.S., Lama, R.D., and Saluja, S.S., 1974, Handbook on mechanical properties of rocks, Volume 1: Testing techniques and results: Bay Village, Ohio, Transactions of Technical Publishers, p. 105–115.
Whipple, K.X, and Tucker, G.E., 1999, Dynamics of the stream-power river incision model: Implications for height limits of mountain ranges, landscape response timescales, and research needs: Journal of Geophysical Research, v. 104, p. 17,661–17,674, doi: 10.1029/1999JB900120.
Whipple, K.X, and Tucker, G.E., 2002, Implications of sediment-flux–dependent river incision models for landscape evolution: Journal of Geophysical Research, v. 107, no. B2, 2039, doi: 10.1029/2000JB000044.
Whipple, K.X, Kirby, E., and Brocklehurst, S.H., 1999, Geomorphic limits to climate-induced increases in topographic relief: Nature, v. 401, p. 39–43, doi: 10.1038/43375.
Whipple, K.X, Snyder, N.P., and Dollenmayer, K., 2000, Rates and processes of bedrock incision by the Upper Ukak River since the 1912 Novarupta ash flow in the Valley of Ten Thousand Smokes, Alaska: Geology, v. 28, p. 835–838, doi: 10.1130/0091-7613(2000)0282.3.CO:2.
Willett, S.D., Slingerland, R., and Hovius, N., 2001, Uplift, shortening, and steady state topography in active mountain belts: American Journal of Science, v. 301, p. 455–485.
Yamaguchi, H., Yoshida, K., Kuroshima, I., and Fukuda, M., 1988, Slaking and shear properties of mudstone, *in* Romana, M., ed., Rock mechanics and power plants: Rotterdam, Balkema, p. 133–144.

Manuscript Received by the Society 9 January 2004
Revised Manuscript Received 6 May 2004
Manuscript Accepted 10 May 2004

Printed in the USA